

Pseudo Redshifts of Gamma-Ray Bursts Derived from the $L - T - E$ Correlation

CHEN DENG (邓晨),¹ YONG-FENG HUANG (黄永峰),^{1,2} AND FAN XU (许帆)¹

¹*School of Astronomy and Space Science, Nanjing University
 Nanjing 210023, People's Republic of China*

²*Key Laboratory of Modern Astronomy and Astrophysics (Nanjing University)
 Ministry of Education, People's Republic of China*

ABSTRACT

The X-ray afterglow of many gamma-ray bursts (GRBs) exhibits a plateau phase before the normal power-law decay stage, which may be related to continued activities of the central engine. Tang et al. (2019) collected 174 such GRBs and confirmed the so called $L - T - E$ correlation which involves three key parameters, i.e., the isotropic γ -ray energy $E_{\gamma,\text{iso}}$ of the prompt phase, the end time T_a of the plateau phase and the corresponding X-ray luminosity L_X . In this study, the $L - T - E$ correlation is confirmed and updated as $L_X \propto T_a^{-0.99} E_{\gamma,\text{iso}}^{0.86}$ with a large sample consisting of 210 plateau GRBs with known redshifts. The tight correlation is then applied to derive the pseudo redshift of other 130 plateau GRBs whose redshifts are not directly measured. Statistical analysis is also carried out on this pseudo redshift sample.

Keywords: Gamma-ray bursts (629); Magnetars (992); Neutron stars (1108); Markov Chain Monte Carlo (1889)

1. INTRODUCTION

Gamma-ray bursts (GRBs) are one of the most powerful stellar explosions in our Universe with the redshifts measured up to $z \sim 9$ (Cucchiara et al. 2011; Salvaterra et al. 2012). In view of this, GRBs are a hopeful tool to probe high-redshift universe (Amati & Della Valle 2013). The spectra of GRBs are generally nonthermal and can be fitted well with the so-called Band function (Band et al. 1993). Traditionally, GRBs can be roughly classified into long ($T_{90} > 2$ s) and short ($T_{90} < 2$ s) categories by their duration T_{90} (defined as the time interval during which 5% — 95% of the prompt γ -ray photons are detected) (Kouveliotou et al. 1993). Long GRBs typically have a duration of 20 — 30 s, while short GRBs usually last for 0.2 — 0.3 s. It is widely believed that long GRBs originate from the death of massive stars (Woosley 1993; MacFadyen & Woosley 1999; Galama et al. 1998; Hjorth et al. 2003; Campana et al. 2006), and short GRBs originate from the merger of binary compact stars (Paczynski 1986; Eichler et al. 1989; Nakar 2007). A recent breakthrough in the field is the detection by the advanced Laser Interferometer Gravitational Wave Observatory of the gravitational-wave event GW 170817 from a binary neutron star merger, which is in association with the short burst GRB 170817A (Abbott et al. 2017). Nevertheless, Norris & Bonnell (2006) found a class of short bursts with extended emission that share some of the properties of both long and short GRBs. Long-duration GRB 211211A, associated with a kilonova, exhibits three components in the prompt phase, also challenging our understanding of

Corresponding author: Yong-Feng Huang
 hyf@nju.edu.cn

GRBs (Rastinejad et al. 2022; Gao et al. 2022). Note that the duration of GRBs is related to the energy band of the detector (Bromberg et al. 2013). In other words, the duration measured by different detectors could be different even for the same burst. Instead of phenomenological classification based on the duration, Zhang (2006) suggested physically classifying GRBs into two different categories, compact star type (type I) and massive star type (type II).

The emission process of GRBs can be divided into two phenomenological phases, namely, the prompt phase and the afterglow phase. The “fireball” model is the most popular mechanism engaged to explain the origin of prompt GRB emission (Rees & Meszaros 1992; Piran et al. 1993 ; Wijers et al. 1997). The central engine, as a result of either the death of a supermassive star or the merge of binary neutron stars, releases a sequence of relativistic shells with different velocities. The collisions of various shells accelerate electrons to produce complex and rapidly changing light curve in the prompt GRB phase, while the interaction of the combined materials with the ambient medium generates the multi-band afterglow at late stages (Mészáros & Rees 1997; Waxman 1997; Sari 1997; Sari et al. 1998; Panaiteescu et al. 1998; Huang et al. 1999, 2000; Yi et al. 2020). Thanks to the rapid response and precise positioning of the Swift satellite, various intricate features have been discovered in GRB afterglows (Burrows et al. 2005; Nousek et al. 2006; O’Brien et al. 2006). A portion of the observed afterglow light curves favor the scenario involving continued late-time energy injection by the central engine (Willingale et al. 2007). As the observational data accumulated, a picture of the canonical afterglow lightcurves consisting of five segments was established (Zhang et al. 2006). The plateau phase usually follows the steep decay phase and is characterized by a shallow temporal decay index (~ 0), which is a common phenomenon in the Swift GRBs (Xu & Huang 2012; Tang et al. 2019). The physical mechanism behind the plateau phase may be the continuous activity of the central engine (Kumar et al. 2008; Cannizzo & Gehrels 2009; Xu & Huang 2012; Yi et al. 2022). A shallow decay phase followed by very steep decay phase with a power-law temporal index < -3 is called an internal plateau (Nousek et al. 2006; Dainotti et al. 2011a; Dainotti & Del Vecchio 2017; Xu et al. 2021, which may be due to the switching off of the energy injection after the supramassive neutron star collapses into a black hole (Chen & Beloborodov 2007; Hou et al. 2018).

GRBs can serve as a probe of the distant universe because of their extreme luminosities(Ghirlanda et al. 2006; Cardone et al. 2009, 2010; Dainotti et al. 2013a; Amati & Della Valle 2013; Postnikov et al. 2014; Dainotti & Del Vecchio 2017; Xu et al. 2021; Hu et al. 2021; Muccino et al. 2021; Wang et al. 2022; Cao et al. 2022; Hu & Wang 2022). Since GRBs may be produced by more than one kind of central engines, the intrinsic energy release of GRBs spans in a wide range, i.e., from $\sim 10^{48}$ erg up to $\sim 10^{55}$ erg (Kumar & Zhang 2015). As a result, GRBs cannot directly serve as a standard candle. Luckily, several tight empirical correlations have been established among various observational parameters of GRBs, which may effectively help alleviate this problem. These correlations usually involve two or more quantities, and can be classified as prompt parameter correlations (Norris et al. 2000; Amati et al. 2002; Ghirlanda et al. 2004, 2006; Yonetoku et al. 2004; Willingale et al. 2007; Dainotti & Amati 2018; Dainotti et al. 2018), afterglow parameter correlations (Dainotti et al. 2008, 2010; Ghisellini et al. 2009), and prompt-afterglow correlations (Liang & Zhang 2005; Xu & Huang 2012; Bernardini et al. 2012; Izzo et al. 2015; Dainotti et al. 2016, 2022a; Si et al. 2018; Tang et al. 2019; Xu et al. 2021). These powerful empirical correlations can not only deepen our understanding of the physical mechanism of GRBs but also act as theoretical model discriminators (Dainotti & Del Vecchio 2017; Dainotti & Amati 2018).

Most of the detected GRBs do not have a measured redshift, which prevents their application in cosmology to some extent. It is interesting to note that some authors have attempted to use empirical correlations to derive pseudo redshifts of GRBs (Atteia 2003; Yonetoku et al. 2004; Dainotti et al. 2011a; Tsutsui et al. 2013; Tan et al. 2013). For example, Tsutsui et al. (2013) calculated the pseudo redshifts of 71 bright short GRBs using a tight $L_p - E_p$ correlation. More recently, Zhang & Wang (2018) used the $L_p - E_p$ correlation to explore the luminosity function and formation rate of short GRBs. In addition, some authors investigated the evolution of the luminosity function and formation rate

in detail for short and long GRBs (Wanderman & Piran 2015; Paul 2018; Dainotti et al. 2021). Following Zhang & Wang (2018), Zitouni et al. (2018) estimated the pseudo redshifts of 1017 Fermi GRBs and investigated their intrinsic duration distribution in the GRB rest frame.

For GRBs with a plateau phase in the X-ray afterglow light curve, Dainotti et al. (2008) firstly discovered an anti-relation between the plateau end time T_a and the corresponding X-ray luminosity L_X using 33 long GRBs detected by the Swift satellite. Consequently, they used this $L_X - T_a$ correlation to estimate pseudo redshifts of GRBs and pointed out that the results are significantly affected by the uncertainty of the observed quantities as well as the intrinsic dispersion of the empirical correlation (Dainotti et al. 2011a). Subsequently, the $L_X - T_a$ relation was extended to a three-parameter correlation among $L_X - T_a - L_p$ by using 40 golden GRBs, where L_p is the peak luminosity of GRBs (Dainotti et al. 2016). Furthermore, the platinum sample consisting of 47 GRBs, as an improvement of the golden sample in the previous study, was used to derive a tighter $L_X - T_a - L_p$ correlation (Dainotti et al. 2017a, 2020a). More elaborate problems in the $L_X - T_a$ correlation and its extensions, such as selection effects and redshift evolution, have been adequately discussed (Dainotti et al. 2013b, 2015a,b, 2017a,b, 2020a, 2022a). On the other hand, Xu & Huang (2012) introduced the prompt isotropic γ -ray energy ($E_{\gamma,\text{iso}}$) as a third key parameter and obtained a tight three-parameter correlation among $L_X - T_a - E_{\gamma,\text{iso}}$ (it is called the $L - T - E$ correlation hereafter). Tang et al. (2019) further collected a large sample consisting of 174 GRBs and confirmed the existence of the $L - T - E$ correlation, e.g., $L_X \propto T_a^{-1.01} E_{\gamma,\text{iso}}^{0.85}$. It is interesting to note that the sample of Tang et al. (2019) includes 6 short GRBs and 11 internal plateau GRBs. They all satisfy the same $L - T - E$ correlation as long GRBs.

Recently, the $L - T - E$ correlation was further confirmed in an independent study by Ding et al. (2022) with a slightly expanded GRB sample. Izzo et al. (2015) derived the Combo-relation as $L_X \propto E_p^{0.84 \pm 0.08} (T_a / |1 + \alpha|)^{-1}$ and argued that there is no redshift evolution in it. Subsequently, some authors proved that the Combo-relation can be used to probe the universe (Luongo & Muccino 2020, 2021; Muccino et al. 2021). Srinivasaragavan et al. (2020) utilized the plateau GRBs to study the closure relations between the temporal and spectral indices in the afterglow phase and showed that the external shock model is generally favored in most cases. More interestingly, there are also two-parameter correlations in the optical afterglow plateau (Zaninoni et al. 2013; Dainotti et al. 2020b). Based on these studies, some three-parameter correlations in optical afterglow phase were established recently (Si et al. 2018; Dainotti et al. 2022b). For comprehensive reviews on the statistics of the plateau phase in GRB afterglows, please refer to Dainotti & Del Vecchio (2017), Dainotti et al. (2018), Zhao et al. (2019) and Wang et al. (2020).

In this study, we will use the $L - T - E$ correlation to estimate the redshifts of GRBs. The structure of our paper is organized as follow. Section 2 describes the sample collection process and some necessary data analysis. The $L - T - E$ correlation is then revisited for plateau GRBs with our sample in Section 3. Pseudo redshifts are calculated for a large number of GRBs based on the $L - T - E$ correlation in Section 4, and the distributions of several derived parameters are also analyzed. Finally, the results are briefly summarized and discussed in Section 5.

2. SAMPLE SELECTION AND DATA ANALYSIS

The shallow decay (plateau) phase is a common phenomenon in the afterglow of GRBs. In this study, we concentrate on the plateau phase in the X-ray afterglow of GRBs and attempt to utilize the $L_X - T_a - E_{\gamma,\text{iso}}$ correlation as a redshift indicator. This so called $L - T - E$ correlation was originally proposed by Xu & Huang (2012). Tang et al. (2019) collected a large sample including 174 GRBs with well defined redshifts and confirmed that the correlation does exist. Here we will first upgrade the $L - T - E$ correlation by using an updated GRB sample containing as many events as possible, which is then utilized to calculate the pseudo redshift of other plateau GRBs without a distance measurement. For this purpose, we have constructed two GRB samples, one with the redshift measured (designated as the Starting Sample), and the other without redshift measurement (designated as the Target Sample). In both samples, each GRB is characterized by an obvious plateau phase in the X-ray afterglow light curve.

The criteria used by Tang et al. (2019) to select the sample are fairly strict, which is very important to clearly define a plateau phase. Following almost the same criteria as Tang et al. (2019), we have re-examined all the GRBs observed by Swift between 2005 March and 2022 May (Evans et al. 2007; Evans et al. 2009). To be more specific, our criteria are: (1) there should be a clear plateau phase in the X-ray afterglow light curve with the temporal

power-law decay index being in the range of -1 to 1 ; (2) Abundant data points are available to well define the plateau phase. (3) The redshifts of the GRBs samples should be well-defined so that we can calculate the isotropic emission energy and luminosity. To expand the sample size as far as possible, we have included those GRBs with X-ray flares superposed on the plateau phase. In these cases, the X-ray flares are simply omitted when fitting the light curve of the plateau phase. As a result, our Starting Sample with known redshift includes 210 GRBs. Comparing with the sample of Tang et al. (2019), 36 GRBs are new in our data set. For GRBs without a redshift measurement, our Target Sample contains 130 events. Pseudo redshift will be calculated for these Target Sample events based on the updated $L - T - E$ correlation. The X-ray light curves of all the GRBs in our two samples have been downloaded from the Swift light curve repository (Evans et al. 2007; Evans et al. 2009).

The plateau phase and the subsequent normal decay phase are then fitted by a smoothly broken power-law function, which is (Yi et al. 2016; Tang et al. 2019)

$$F_X(t) = F_{X0} \left[\left(\frac{t}{T_{a,\text{obs}}} \right)^{\alpha_1 \omega} + \left(\frac{t}{T_{a,\text{obs}}} \right)^{\alpha_2 \omega} \right]^{-1/\omega}, \quad (1)$$

where α_1 , α_2 , $T_{a,\text{obs}}$ and ω represent the temporal power-law decay index of the plateau phase, the decay index of the post-break segment, the break time in the observer's frame, and the smoothness factor of the transition segment, respectively. The end time of the plateau in the GRB rest frame can be obtained by $T_a = T_{a,\text{obs}}/(1+z)$. The flux at the break time is $F_{X0} \times 2^{-1/\omega}$. For simplicity, the smoothness factor is fixed as 1.0 in our fitting process. Correspondingly, the flux at the end of the plateau phase is $F_{X0}/2$.

The Markov Chain Monte Carlo (MCMC) algorithm is employed to fit the GRB afterglow light curves. The key parameters derived in the fitting process are presented in Table 1 and Table 2 for the Starting Sample and the Target Sample, respectively. An example showing our best fit to the plateau phase and the subsequent X-ray light curve of GRB 190106A is illustrated in Figure 1.

After obtaining these key parameters, the isotropic luminosity at the end time of the plateau phase can then be calculated as

$$L_X = 4\pi D_L^2(z) \frac{F_{X0}}{2} K, \quad (2)$$

where $D_L(z)$ is the luminosity distance, i.e.,

$$D_L(z) = (1+z) \frac{C}{H_0} \int_0^z \frac{dz'}{\sqrt{\Omega_M(1+z')^3 + \Omega_\Lambda}}, \quad (3)$$

where z is the redshift and C is the speed of light. In this study, a flat Λ CDM cosmology with parameters of $H_0 = 70.0 \text{ km s}^{-1} \text{ Mpc}^{-1}$, $\Omega_M = 0.286$ and $\Omega_\Lambda = 1 - \Omega_M$ is adopted. Meanwhile, the K -correction is considered in our calculations, which is (Bloom et al. 2001)

$$K = \frac{\int_{E_1/(1+z)}^{E_2/(1+z)} EN(E)dE}{\int_{E_1}^{E_2} EN(E)dE}, \quad (4)$$

where (E_1, E_2) stands for the energy band of the detector. Equation (4) of Schaefer (2007) gives a general form of the GRB photon spectrum. Considering the relatively narrow energy bandpass of XRT onboard Swift, we adopt a simple

power-law function for the photon spectrum, e.g., $N(E) = N_0 E^{-\beta_X}$, where N_0 is a normalization coefficient and β_X is the photon index measured by Swift XRT. Consequently, the isotropic X-ray luminosity at the break time is

$$L_X = \frac{4\pi D_L^2(z)}{(1+z)^{2-\beta_X}} \frac{F_{X0}}{2}, \quad (5)$$

after the K -correction.

Similarly, the isotropic γ -ray energy of the prompt phase (after K -correction) is calculated as

$$E_{\gamma,\text{iso}} = \frac{4\pi D_L^2(z)S}{(1+z)} K = \frac{4\pi D_L^2(z)S}{(1+z)^{3-\alpha_\gamma}}, \quad (6)$$

where S and α_γ are the fluence and the photon spectral index measured by Swift/BAT, respectively. The parameters of α_γ and β_X are taken from the Swift GRB database ¹.

A preliminary analyse has been carried out on the basic features of these two samples. Figure 2 presents the distributions of the plateau flux (F_X , 0.3 — 10 keV), the Swift/BAT fluence (S , 15 — 150 keV) and the duration (T_{90}). For the Starting Sample, we see that the mean values of F_X , S , and T_{90} are $0.8 \times 10^{-11} \text{ erg cm}^{-2} \text{ s}^{-1}$, $2.04 \times 10^{-6} \text{ erg cm}^{-2}$ and 39.8 s, respectively. Correspondingly, for the Target Sample, the mean values of F_X , S , and T_{90} are $1.2 \times 10^{-11} \text{ erg cm}^{-2} \text{ s}^{-1}$, $2.69 \times 10^{-6} \text{ erg cm}^{-2}$ and 47.9 s, respectively. We see that the distributions of these three parameters are largely similar for the two samples, indicating that there is no systematic difference between them. The distributions of the temporal power-law decay indices of the plateau phase (α_1) and the post-break segment (α_2) are shown in Figure 3. The mean values of α_1 are 0.19 and 0.24 for the Starting Sample and the Targeting Sample, respectively. Correspondingly, the mean values of α_2 are 1.77 and 1.68 for them. Again, we see that the distributions of α_1 and α_2 are similar for the two samples.

3. THE L – T – E CORRELATION UPDATED

Tang et al. (2019) derived the $L – T – E$ correlation as $L_X \propto T_a^{-1.01} E_{\gamma,\text{iso}}^{0.85}$ with a sample of 174 GRBs. In this section, we utilize our expanded sample, i.e. the Starting Sample, which includes 210 GRBs, to further study the $L – T – E$ correlation. To begin with, let us write down the three parameter correlation in a general form of (Xu & Huang 2012; Tang et al. 2019)

$$\log(L_X/10^{47} \text{ erg s}^{-1}) = a + b \log(T_a/10^3 \text{ s}) + c \log(E_{\gamma,\text{iso}}/10^{53} \text{ erg}), \quad (7)$$

where, a , b , and c are coefficients to be determined through observational data. For each GRB, the parameters of L_X , T_a , and $E_{\gamma,\text{iso}}$ can be taken from Table 1.

An MCMC algorithm is utilized to fit the observational data to derive the updated $L – T – E$ correlation. To do so, we adopt a joint likelihood function that is widely used in multi-parameter fitting process, i.e. (D’Agostini 2005)

$$\mathcal{L}(a, b, c, \sigma_{\text{int}}) \propto \prod_n \frac{1}{\sqrt{\sigma_{\text{int}}^2 + \sigma_{y,n}^2 + b^2 \sigma_{x_{1,n}}^2 + c^2 \sigma_{x_{2,n}}^2}} \exp \left[-\frac{(y_n - a - bx_{1,n} - cx_{2,n})^2}{2(\sigma_{\text{int}}^2 + \sigma_{y,n}^2 + b^2 \sigma_{x_{1,n}}^2 + c^2 \sigma_{x_{2,n}}^2)} \right], \quad (8)$$

where n is the sample size and σ_{int} represents possible intrinsic scatter caused by some unknown variables. In our calculations, y , x_1 and x_2 represent $\log(L_X/10^{47} \text{ erg s}^{-1})$, $\log(T_a/10^3 \text{ s})$ and $\log(E_{\gamma,\text{iso}}/10^{53} \text{ erg})$, respectively. σ_y , σ_{x_1} and σ_{x_2} are the corresponding error bars.

For the 210 GRBs in the Starting Sample, the best-fit $L – T – E$ correlation is

$$\log(L_X/10^{47} \text{ erg s}^{-1}) = (1.61 \pm 0.05) + (-0.99 \pm 0.04) \times \log(T_a/10^3 \text{ s}) + (0.86 \pm 0.04) \times \log(E_{\gamma,\text{iso}}/10^{53} \text{ erg}). \quad (9)$$

¹ https://swift.gsfc.nasa.gov/archive/grb_table/

The fitting results are illustrated in Figure 4. We see that Equation (9) is well consistent with previous results of Tang et al. (2019), who derived the correlation as $L_X \propto T_a^{-1.01} E_{\gamma,\text{iso}}^{0.85}$, with $\sigma_{\text{int}} = 0.40 \pm 0.03$. Our study further confirms the existence of the $L - T - E$ correlation. Note that our intrinsic scatter parameter is $\sigma_{\text{int}} = 0.36 \pm 0.03$, which is slightly smaller than that obtained by Tang et al. (2019). It means that the correlation is even tighter for this expanded sample.

4. PSEUDO REDSHIFTS FROM THE $L - T - E$ CORRELATION

The three-parameter $L - T - E$ correlation connects redshift with the observed quantities of S (the fluence), T_a , and F_X (the X-ray flux). It hints us that we could employ the correlation to estimate the redshift for GRBs in the Target Sample, whose redshifts are all unknown. For this purpose, we first define a function $g(z)$ as

$$\begin{aligned} g(z) &= \log(L_X/10^{47}\text{erg s}^{-1}) - a - b \log(T_a/10^3\text{s}) - c \log(E_{\gamma,\text{iso}}/10^{53}\text{erg}) \\ &= (2 - 2c) \log \left(\int_0^z \frac{1}{\sqrt{(1+z')^3 \Omega_M + \Omega_\Lambda}} dz' \right) + (b + c + \beta_X - c\alpha_\gamma) \log(1+z) \\ &\quad - c \log(4\pi S) + \log(2\pi F_{X0}) - a - b \log(T_{a,\text{obs}}) + 3b - 47 + 53c + (2 - 2c) \log \left(\frac{C}{H_0} \right). \end{aligned} \quad (10)$$

In our calculations, the best fitting values derived in Section 3 are adopted for the coefficients a , b and c , e.g. $a = 1.61$, $b = -0.99$ and $c = 0.86$.

If a particular GRB strictly satisfies the $L - T - E$ correlation, then the corresponding $g(z)$ should be zero. So we can calculate the pseudo redshift of a GRB by solving the equation of $g(z) = 0$ when the F_X , S , $T_{a,\text{obs}}$, α_γ , β_X parameters are available. In other words, the pseudo redshift is the intersection of the function $g(z)$ with the horizontal axis in the $g(z) - z$ plane. As a demonstration, the function $g(z)$ is plot for all target GRBs in Figure 5. We can see that the $g(z)$ curve is generally very flat at high redshift. In fact, if the intersection is at a point with $z > 20$, the derived pseudo redshift will be highly uncertain due to the existence of the error bars of the input parameters, i.e. F_X , S , $T_{a,\text{obs}}$, α_γ , and β_X . So, in our calculations, we will limit the valid range of the pseudo redshift in $0 < z < 20$. It should also be noted that for a small fraction ($\sim 1/6$) of the target GRBs, the $g(z)$ curve is well under the zero line up to $z = 20$. It means that these GRBs may have a redshift larger than 20. However, the possibility that they actually do not follow the $L - T - E$ correlation cannot be excluded.

Using the three-parameter $L - T - E$ correlation, we have tried to calculate the pseudo redshifts for GRBs in the Target Sample. Due to the reason mentioned just above, the redshift can be derived only for 108 target GRBs. For the remaining 22 GRBs in the sample, the pseudo redshift is not available.

With the pseudo redshift, we can then calculate some key parameters of the target GRBs, such as $E_{\gamma,\text{iso}}$, L_X , and T_a (note that this break time is defined in the GRB rest frame), which are all distance-dependent. Figure 6 shows the distributions of these derived parameters, together with that of z . For the Target Sample, the mean values of $E_{\gamma,\text{iso}}$, L_X , z and T_a are $6.46 \times 10^{51}\text{erg}$, $1.82 \times 10^{47}\text{erg s}^{-1}$, 3.08 and $2.14 \times 10^3\text{s}$, respectively. As a comparison, for the Starting Sample, the corresponding mean values are $8.91 \times 10^{51}\text{erg}$, $1.91 \times 10^{47}\text{erg s}^{-1}$, 2.2 and $2.51 \times 10^3\text{s}$, respectively. We see that the distributions of these parameters are quite similar for the two samples. The largest difference is observed in the distribution of z . The mean distance of Target Sample is obviously higher than that of the Starting Sample. This is mainly due to the fact that a few target GRBs have a very high pseudo redshift, larger than 10. Whether these events really reside at such high redshifts is an interesting question.

If the pseudo redshift is really a credible measure of the distance of the GRBs, then it is interesting to examine whether the Target Sample also satisfy other popular correlations of GRBs. Let us first take the $L_X - T_a$ correlation as an example. Dainotti et al. (2008) discovered for the first time that there is an anti-correlation between L_X and

T_a . The effects of selection bias and redshift evolution on the $L_X - T_a$ correlation have been investigated in previous studies (Dainotti et al. 2013b, 2015a, 2017b, 2022a). Here we take the power-law evolutionary functions proposed by Dainotti et al. (2022a), e.g., $G(z) = (1+z)^{k_{L_X}}$ and $F(z) = (1+z)^{k_{T_a}}$. The local variables are defined as $L'_X \equiv L_X/G(z)$ and $T'_a \equiv T_a/F(z)$. The power-law indices, k_{L_X} and k_{T_a} , are 2.42 ± 0.58 and -1.25 ± 0.28 . In Figure 7(a), L'_X is plot against T'_a for the Target Sample, and the results are compared with that of normal GRBs with a measured redshift. For normal GRBs, the best fit $L'_X - T'_a$ relation is $L'_X \propto T_a^{-0.93 \pm 0.08}$, and it is $L'_X \propto T_a^{-0.87 \pm 0.14}$ for the Target Sample. These results are consistent with Dainotti et al. (2017b). We see that these two groups are well consistent with each other. In fact, most of the target GRBs fall within the $2\sigma_{\text{int}}$ range of normal GRBs.

Another interesting example is the prompt-afterglow $L_X - \bar{L}_{\gamma,90}$ correlation (Dainotti et al. 2011b, 2015a). Here $\bar{L}_{\gamma,90}$ is defined as $\bar{L}_{\gamma,90} \equiv E_{\gamma,\text{iso}}(1+z)/T_{90}$, which reflects the average intrinsic luminosity of the prompt emission phase. Figure 7(b) plots L_X versus $\bar{L}_{\gamma,90}$ for the two GRB groups. We see that there is an obvious correlation between L_X and $\bar{L}_{\gamma,90}$ for each group. However, the best fit result is $\bar{L}_{\gamma,90} \propto L_X^{0.98 \pm 0.04}$ for the Target Sample, while it is $\bar{L}_{\gamma,90} \propto L_X^{0.53 \pm 0.03}$ for normal GRBs. There is a clear difference in the power-law index. The reason of this difference is still unknown and deserves further studying in the future.

As mentioned above, the pseudo redshift could not be derived for 22 GRBs in the Target Sample. Here we present some detailed discussion on this issue. In Equation (10), we notice that the coefficient of the item $\log(1+z)$ is $b + c + \beta_X - c\alpha_\gamma$. Since $b \sim -1$ and $c \sim 1$ in our cases, the exact value of this coefficient is mainly determined by $\beta_X - \alpha_\gamma$. If $\beta_X \approx \alpha_\gamma$, then there will be a singular point in the function so that the pseudo redshift could not be solved. To further examine this issue, the photon indices of the Target Sample are plot in Figure 8, where the 22 GRBs are specially marked by star symbols. In Figure 8(a), we see that the distribution of these 22 events does deviate from the other GRBs systematically. Especially, Figure 8(b) clearly shows that the mean value of $\beta_X - \alpha_\gamma$ is very close to zero for these 22 GRBs. This is exactly the reason that their pseudo redshift cannot be derived.

5. SUMMARY AND DISCUSSION

Many GRBs are characterized by a plateau phase in the X-ray afterglow light curve. In this study, we have collected a large sample containing 210 such GRBs with known redshifts. With this Starting Sample, the three parameter $L - T - E$ correlation is updated as $L_X \propto T_a^{-0.99 \pm 0.04} E_{\gamma,\text{iso}}^{0.86 \pm 0.04}$, which is consistent with the results of Xu & Huang (2012) and Tang et al. (2019). We have also collected another sample, i.e. the Target Sample, which contains 130 plateau GRBs whose redshifts were not measured. It is found that the distributions of many key parameters are similar for the two samples. The upgraded $L - T - E$ correlation is then applied to the Target Sample. Pseudo redshifts are calculated for 108 GRBs in this sample. But for the remaining 22 GRBs, the pseudo redshift cannot be credibly derived. The reason may be that they are either at extremely high redshifts or they do not strictly follow the $L - T - E$ correlation. It could also be due to the fact that they have an equal photon index in X-rays and γ -rays, i.e. $\alpha_\gamma \approx \beta_X$.

The origin of the plateau phase in the X-ray afterglow of GRBs is still quite uncertain. Suvorov & Kokkotas (2021) argued that it could not be produced by the fall-back accretion of a black hole because of the short surviving time-scale (\sim seconds). In fact, the most popular interpretation is that it is due to the energy injection from a millisecond magnetar, through dipolar radiation (Duncan & Thompson 1992; Dall’Osso et al. 2011; Rea et al. 2015; Stratta et al. 2018). The anti-correlation of $L_X - T_a$ and the three parameter $L - T - E$ correlation are all argued to be clues supporting this mechanism (Dainotti et al. 2008; Xu & Huang 2012; Tang et al. 2019). According to this study, the upgraded $L - T - E$ correlation is $L_X \propto T_a^{-0.99} E_{\gamma,\text{iso}}^{0.86}$. Note that the power-law index of T_a is close to -1 and the index of $E_{\gamma,\text{iso}}$ is close to 1 . In other words, the correlation indicates $L_X T_a \propto E_{\gamma,\text{iso}}$. Since $E_{\gamma,\text{iso}}$ itself is closely connected to the initial spin energy of the millisecond magnetar, we see that the $L - T - E$ correlation does support such an explanation for the plateau phase. Note that the emergence of quasi-periodic oscillation signatures in the plateau

phase, which may be due to the precessing of a neutron star, provides further support for this mechanism (Suvorov & Kokkotas 2021; Zou & Liang 2022).

Pseudo redshifts are reasonable estimate for the distances of GRBs whose spectral redshifts were not measured. Especially, they are useful for some statistical studies (Zitouni et al. 2018). Note that the accuracy of the pseudo redshifts could be affected by many factors, such as the error bars of the input parameters (i.e. F_X , S , $T_{\text{a,obs}}$, α_γ , β_X), the intrinsic scatter of the $L - T - E$ correlation, and even possible deviation from the $L - T - E$ correlation by the target GRB itself. Reducing the intrinsic dispersion (σ_{int}) of the empirical correlation could help improve the reliability of the pseudo redshifts (Dainotti et al. 2011a). Dainotti et al. (2011b) have built a gold sample to try to derive a more compact relation, which is obviously a meaningful exploration. More studies could be carried out in this aspect in the future.

ACKNOWLEDGEMENTS

This study is supported by the National Natural Science Foundation of China (Grant Nos. 12233002, 11873030, 12041306, 12147103, U1938201), by National SKA Program of China No. 2020SKA0120300, by the National Key R&D Program of China (2021YFA0718500), and by the science research grants from the China Manned Space Project with NO. CMS-CSST-2021-B11. This work made use of data supplied by the UK Swift Science Data Center at the University of Leicester.

REFERENCES

- Abbott, B. P., Abbott, R., Abbott, T. D., et al. 2017, ApJL, 848, L13, doi: [10.3847/2041-8213/aa920c](https://doi.org/10.3847/2041-8213/aa920c)
- Amati, L., & Della Valle, M. 2013, International Journal of Modern Physics D, 22, 1330028, doi: [10.1142/S0218271813300280](https://doi.org/10.1142/S0218271813300280)
- Amati, L., Frontera, F., Tavani, M., et al. 2002, A&A, 390, 81, doi: [10.1051/0004-6361:20020722](https://doi.org/10.1051/0004-6361:20020722)
- Atteia, J. L. 2003, A&A, 407, L1, doi: [10.1051/0004-6361:20030958](https://doi.org/10.1051/0004-6361:20030958)
- Band, D., Matteson, J., Ford, L., et al. 1993, ApJ, 413, 281, doi: [10.1086/172995](https://doi.org/10.1086/172995)
- Bernardini, M. G., Margutti, R., Zaninoni, E., & Chincarini, G. 2012, MNRAS, 425, 1199, doi: [10.1111/j.1365-2966.2012.21487.x](https://doi.org/10.1111/j.1365-2966.2012.21487.x)
- Bloom, J. S., Frail, D. A., & Sari, R. 2001, AJ, 121, 2879, doi: [10.1086/321093](https://doi.org/10.1086/321093)
- Bromberg, O., Nakar, E., Piran, T., & Sari, R. 2013, ApJ, 764, 179, doi: [10.1088/0004-637X/764/2/179](https://doi.org/10.1088/0004-637X/764/2/179)
- Burrows, D. N., Romano, P., Falcone, A., et al. 2005, Science, 309, 1833, doi: [10.1126/science.1116168](https://doi.org/10.1126/science.1116168)
- Campana, S., Mangano, V., Blustin, A. J., et al. 2006, Nature, 442, 1008, doi: [10.1038/nature04892](https://doi.org/10.1038/nature04892)
- Cannizzo, J. K., & Gehrels, N. 2009, ApJ, 700, 1047, doi: [10.1088/0004-637X/700/2/1047](https://doi.org/10.1088/0004-637X/700/2/1047)
- Cao, S., Dainotti, M., & Ratra, B. 2022, MNRAS, 512, 439, doi: [10.1093/mnras/stac517](https://doi.org/10.1093/mnras/stac517)
- Cardone, V. F., Capozziello, S., & Dainotti, M. G. 2009, MNRAS, 400, 775, doi: [10.1111/j.1365-2966.2009.15456.x](https://doi.org/10.1111/j.1365-2966.2009.15456.x)
- Cardone, V. F., Dainotti, M. G., Capozziello, S., & Willingale, R. 2010, MNRAS, 408, 1181, doi: [10.1111/j.1365-2966.2010.17197.x](https://doi.org/10.1111/j.1365-2966.2010.17197.x)
- Chen, W.-X., & Beloborodov, A. M. 2007, ApJ, 657, 383, doi: [10.1086/508923](https://doi.org/10.1086/508923)
- Cucchiara, A., Levan, A. J., Fox, D. B., et al. 2011, ApJ, 736, 7, doi: [10.1088/0004-637X/736/1/7](https://doi.org/10.1088/0004-637X/736/1/7)
- D'Agostini, G. 2005, arXiv e-prints, arXiv:physics/0511182, doi: [10.48550/ARXIV.PHYSICS/0511182](https://doi.org/10.48550/ARXIV.PHYSICS/0511182)
- Dainotti, M., Petrosian, V., Willingale, R., et al. 2015a, MNRAS, 451, 3898, doi: [10.1093/mnras/stv1229](https://doi.org/10.1093/mnras/stv1229)
- Dainotti, M. G., & Amati, L. 2018, PASP, 130, 051001, doi: [10.1088/1538-3873/aaa8d7](https://doi.org/10.1088/1538-3873/aaa8d7)
- Dainotti, M. G., Cardone, V. F., & Capozziello, S. 2008, MNRAS, 391, L79, doi: [10.1111/j.1745-3933.2008.00560.x](https://doi.org/10.1111/j.1745-3933.2008.00560.x)
- Dainotti, M. G., Cardone, V. F., Piedipalumbo, E., & Capozziello, S. 2013a, MNRAS, 436, 82, doi: [10.1093/mnras/stt1516](https://doi.org/10.1093/mnras/stt1516)
- Dainotti, M. G., & Del Vecchio, R. 2017, NewAR, 77, 23, doi: [10.1016/j.newar.2017.04.001](https://doi.org/10.1016/j.newar.2017.04.001)
- Dainotti, M. G., Del Vecchio, R., Shigehiro, N., & Capozziello, S. 2015b, ApJ, 800, 31, doi: [10.1088/0004-637X/800/1/31](https://doi.org/10.1088/0004-637X/800/1/31)
- Dainotti, M. G., Del Vecchio, R., & Tarnopolski, M. 2018, Advances in Astronomy, 2018, 4969503, doi: [10.1155/2018/4969503](https://doi.org/10.1155/2018/4969503)

- Dainotti, M. G., Fabrizio Cardone, V., Capozziello, S., Ostrowski, M., & Willingale, R. 2011a, ApJ, 730, 135, doi: [10.1088/0004-637X/730/2/135](https://doi.org/10.1088/0004-637X/730/2/135)
- Dainotti, M. G., Hernandez, X., Postnikov, S., et al. 2017a, ApJ, 848, 88, doi: [10.3847/1538-4357/aa8a6b](https://doi.org/10.3847/1538-4357/aa8a6b)
- Dainotti, M. G., Lenart, A. L., Sarracino, G., et al. 2020a, ApJ, 904, 97, doi: [10.3847/1538-4357/abbe8a](https://doi.org/10.3847/1538-4357/abbe8a)
- Dainotti, M. G., Nagataki, S., Maeda, K., Postnikov, S., & Pian, E. 2017b, A&A, 600, A98, doi: [10.1051/0004-6361/201628384](https://doi.org/10.1051/0004-6361/201628384)
- Dainotti, M. G., Nielson, V., Sarracino, G., et al. 2022a, MNRAS, 514, 1828, doi: [10.1093/mnras/stac1141](https://doi.org/10.1093/mnras/stac1141)
- Dainotti, M. G., Ostrowski, M., & Willingale, R. 2011b, MNRAS, 418, 2202, doi: [10.1111/j.1365-2966.2011.19433.x](https://doi.org/10.1111/j.1365-2966.2011.19433.x)
- Dainotti, M. G., Petrosian, V., & Bowden, L. 2021, ApJL, 914, L40, doi: [10.3847/2041-8213/abf5e4](https://doi.org/10.3847/2041-8213/abf5e4)
- Dainotti, M. G., Petrosian, V., Singal, J., & Ostrowski, M. 2013b, ApJ, 774, 157, doi: [10.1088/0004-637X/774/2/157](https://doi.org/10.1088/0004-637X/774/2/157)
- Dainotti, M. G., Postnikov, S., Hernandez, X., & Ostrowski, M. 2016, ApJL, 825, L20, doi: [10.3847/2041-8205/825/2/L20](https://doi.org/10.3847/2041-8205/825/2/L20)
- Dainotti, M. G., Willingale, R., Capozziello, S., Fabrizio Cardone, V., & Ostrowski, M. 2010, ApJL, 722, L215, doi: [10.1088/2041-8205/722/2/L215](https://doi.org/10.1088/2041-8205/722/2/L215)
- Dainotti, M. G., Livermore, S., Kann, D. A., et al. 2020b, ApJL, 905, L26, doi: [10.3847/2041-8213/abeda9](https://doi.org/10.3847/2041-8213/abeda9)
- Dainotti, M. G., Young, S., Li, L., et al. 2022b, ApJS, 261, 25, doi: [10.3847/1538-4365/ac7c64](https://doi.org/10.3847/1538-4365/ac7c64)
- Dall’Osso, S., Stratta, G., Guetta, D., et al. 2011, A&A, 526, A121, doi: [10.1051/0004-6361/201014168](https://doi.org/10.1051/0004-6361/201014168)
- Ding, X.-K., Shi, Y.-R., Zhu, S.-Y., Sun, W.-P., & Zhang, F.-W. 2022, Ap&SS, 367, 58, doi: [10.1007/s10509-022-04088-9](https://doi.org/10.1007/s10509-022-04088-9)
- Duncan, R. C., & Thompson, C. 1992, ApJL, 392, L9, doi: [10.1086/186413](https://doi.org/10.1086/186413)
- Eichler, D., Livio, M., Piran, T., & Schramm, D. N. 1989, Nature, 340, 126, doi: [10.1038/340126a0](https://doi.org/10.1038/340126a0)
- Evans, P. A., Beardmore, A. P., Page, K. L., et al. 2007, A&A, 469, 379, doi: [10.1051/0004-6361:20077530](https://doi.org/10.1051/0004-6361:20077530)
- Evans, P. A., Beardmore, A. P., Page, K. L., et al. 2009, MNRAS, 397, 1177, doi: [10.1111/j.1365-2966.2009.14913.x](https://doi.org/10.1111/j.1365-2966.2009.14913.x)
- Galama, T. J., Vreeswijk, P. M., van Paradijs, J., et al. 1998, Nature, 395, 670, doi: [10.1038/27150](https://doi.org/10.1038/27150)
- Gao, H., Lei, W.-H., & Zhu, Z.-P. 2022, ApJL, 934, L12, doi: [10.3847/2041-8213/ac80c7](https://doi.org/10.3847/2041-8213/ac80c7)
- Ghirlanda, G., Ghisellini, G., & Firmani, C. 2006, New Journal of Physics, 8, 123, doi: [10.1088/1367-2630/8/7/123](https://doi.org/10.1088/1367-2630/8/7/123)
- Ghirlanda, G., Ghisellini, G., & Lazzati, D. 2004, ApJ, 616, 331, doi: [10.1086/424913](https://doi.org/10.1086/424913)
- Ghisellini, G., Nardini, M., Ghirlanda, G., & Celotti, A. 2009, MNRAS, 393, 253, doi: [10.1111/j.1365-2966.2008.14214.x](https://doi.org/10.1111/j.1365-2966.2008.14214.x)
- Hjorth, J., Sollerman, J., Møller, P., et al. 2003, Nature, 423, 847, doi: [10.1038/nature01750](https://doi.org/10.1038/nature01750)
- Hou, S.-J., Liu, T., Xu, R.-X., et al. 2018, ApJ, 854, 104, doi: [10.3847/1538-4357/aaabba](https://doi.org/10.3847/1538-4357/aaabba)
- Hu, J. P., & Wang, F. Y. 2022, A&A, 661, A71, doi: [10.1051/0004-6361/202142162](https://doi.org/10.1051/0004-6361/202142162)
- Hu, J. P., Wang, F. Y., & Dai, Z. G. 2021, MNRAS, 507, 730, doi: [10.1093/mnras/stab2180](https://doi.org/10.1093/mnras/stab2180)
- Huang, Y. F., Dai, Z. G., & Lu, T. 1999, MNRAS, 309, 513, doi: [10.1046/j.1365-8711.1999.02887.x](https://doi.org/10.1046/j.1365-8711.1999.02887.x)
- Huang, Y. F., Gou, L. J., Dai, Z. G., & Lu, T. 2000, ApJ, 543, 90, doi: [10.1086/317076](https://doi.org/10.1086/317076)
- Izzo, L., Muccino, M., Zaninoni, E., Amati, L., & Della Valle, M. 2015, A&A, 582, A115, doi: [10.1051/0004-6361/201526461](https://doi.org/10.1051/0004-6361/201526461)
- Kouveliotou, C., Meegan, C. A., Fishman, G. J., et al. 1993, ApJL, 413, L101, doi: [10.1086/186969](https://doi.org/10.1086/186969)
- Kumar, P., Narayan, R., & Johnson, J. L. 2008, Science, 321, 376, doi: [10.1126/science.1159003](https://doi.org/10.1126/science.1159003)
- Kumar, P., & Zhang, B. 2015, PhR, 561, 1, doi: [10.1016/j.physrep.2014.09.008](https://doi.org/10.1016/j.physrep.2014.09.008)
- Liang, E., & Zhang, B. 2005, ApJ, 633, 611, doi: [10.1086/491594](https://doi.org/10.1086/491594)
- Luongo, O., & Muccino, M. 2020, A&A, 641, A174, doi: [10.1051/0004-6361/202038264](https://doi.org/10.1051/0004-6361/202038264)
- . 2021, MNRAS, 503, 4581, doi: [10.1093/mnras/stab795](https://doi.org/10.1093/mnras/stab795)
- MacFadyen, A. I., & Woosley, S. E. 1999, ApJ, 524, 262, doi: [10.1086/307790](https://doi.org/10.1086/307790)
- Mészáros, P., & Rees, M. J. 1997, ApJ, 476, 232, doi: [10.1086/303625](https://doi.org/10.1086/303625)
- Muccino, M., Izzo, L., Luongo, O., et al. 2021, ApJ, 908, 181, doi: [10.3847/1538-4357/abd254](https://doi.org/10.3847/1538-4357/abd254)
- Nakar, E. 2007, PhR, 442, 166, doi: [10.1016/j.physrep.2007.02.005](https://doi.org/10.1016/j.physrep.2007.02.005)
- Norris, J. P., & Bonnell, J. T. 2006, ApJ, 643, 266, doi: [10.1086/502796](https://doi.org/10.1086/502796)
- Norris, J. P., Marani, G. F., & Bonnell, J. T. 2000, ApJ, 534, 248, doi: [10.1086/308725](https://doi.org/10.1086/308725)
- Nousek, J. A., Kouveliotou, C., Grupe, D., et al. 2006, ApJ, 642, 389, doi: [10.1086/500724](https://doi.org/10.1086/500724)
- O’Brien, P. T., Willingale, R., Osborne, J., et al. 2006, ApJ, 647, 1213, doi: [10.1086/505457](https://doi.org/10.1086/505457)
- Paczynski, B. 1986, ApJL, 308, L43, doi: [10.1086/184740](https://doi.org/10.1086/184740)
- Panaiteescu, A., Mészáros, P., & Rees, M. J. 1998, ApJ, 503, 314, doi: [10.1086/305995](https://doi.org/10.1086/305995)

- Paul, D. 2018, MNRAS, 473, 3385, doi: [10.1093/mnras/stx2511](https://doi.org/10.1093/mnras/stx2511)
- Piran, T., Shemi, A., & Narayan, R. 1993, MNRAS, 263, 861, doi: [10.1093/mnras/263.4.861](https://doi.org/10.1093/mnras/263.4.861)
- Postnikov, S., Dainotti, M. G., Hernandez, X., & Capozziello, S. 2014, ApJ, 783, 126, doi: [10.1088/0004-637X/783/2/126](https://doi.org/10.1088/0004-637X/783/2/126)
- Rastinejad, J. C., Gompertz, B. P., Levan, A. J., et al. 2022, arXiv e-prints, arXiv:2204.10864. <https://arxiv.org/abs/2204.10864>
- Rea, N., Gullón, M., Pons, J. A., et al. 2015, ApJ, 813, 92, doi: [10.1088/0004-637X/813/2/92](https://doi.org/10.1088/0004-637X/813/2/92)
- Rees, M. J., & Meszaros, P. 1992, MNRAS, 258, 41, doi: [10.1093/mnras/258.1.41P](https://doi.org/10.1093/mnras/258.1.41P)
- Salvaterra, R., Campana, S., Vergani, S. D., et al. 2012, ApJ, 749, 68, doi: [10.1088/0004-637X/749/1/68](https://doi.org/10.1088/0004-637X/749/1/68)
- Sari, R. 1997, ApJL, 489, L37, doi: [10.1086/310957](https://doi.org/10.1086/310957)
- Sari, R., Piran, T., & Narayan, R. 1998, ApJL, 497, L17, doi: [10.1086/311269](https://doi.org/10.1086/311269)
- Schaefer, B. E. 2007, ApJ, 660, 16, doi: [10.1086/511742](https://doi.org/10.1086/511742)
- Si, S.-K., Qi, Y.-Q., Xue, F.-X., et al. 2018, ApJ, 863, 50, doi: [10.3847/1538-4357/aad08a](https://doi.org/10.3847/1538-4357/aad08a)
- Srinivasaragavan, G. P., Dainotti, M. G., Fraija, N., et al. 2020, ApJ, 903, 18, doi: [10.3847/1538-4357/abb702](https://doi.org/10.3847/1538-4357/abb702)
- Stratta, G., Dainotti, M. G., Dall'Osso, S., Hernandez, X., & De Cesare, G. 2018, ApJ, 869, 155, doi: [10.3847/1538-4357/aadd8f](https://doi.org/10.3847/1538-4357/aadd8f)
- Suvorov, A. G., & Kokkotas, K. D. 2021, MNRAS, 502, 2482, doi: [10.1093/mnras/stab153](https://doi.org/10.1093/mnras/stab153)
- Tan, W.-W., Cao, X.-F., & Yu, Y.-W. 2013, ApJL, 772, L8, doi: [10.1088/2041-8205/772/1/L8](https://doi.org/10.1088/2041-8205/772/1/L8)
- Tang, C.-H., Huang, Y.-F., Geng, J.-J., & Zhang, Z.-B. 2019, ApJS, 245, 1, doi: [10.3847/1538-4365/ab4711](https://doi.org/10.3847/1538-4365/ab4711)
- Tsutsui, R., Yonetoku, D., Nakamura, T., Takahashi, K., & Moribara, Y. 2013, MNRAS, 431, 1398, doi: [10.1093/mnras/stt262](https://doi.org/10.1093/mnras/stt262)
- Wanderman, D., & Piran, T. 2015, MNRAS, 448, 3026, doi: [10.1093/mnras/stv123](https://doi.org/10.1093/mnras/stv123)
- Wang, F., Zou, Y.-C., Liu, F., et al. 2020, ApJ, 893, 77, doi: [10.3847/1538-4357/ab0a86](https://doi.org/10.3847/1538-4357/ab0a86)
- Wang, F. Y., Hu, J. P., Zhang, G. Q., & Dai, Z. G. 2022, ApJ, 924, 97, doi: [10.3847/1538-4357/ac3755](https://doi.org/10.3847/1538-4357/ac3755)
- Waxman, E. 1997, ApJL, 485, L5, doi: [10.1086/310809](https://doi.org/10.1086/310809)
- Wijers, R. A. M. J., Rees, M. J., & Meszaros, P. 1997, MNRAS, 288, L51, doi: [10.1093/mnras/288.4.L51](https://doi.org/10.1093/mnras/288.4.L51)
- Willingale, R., O'Brien, P. T., Osborne, J. P., et al. 2007, ApJ, 662, 1093, doi: [10.1086/517989](https://doi.org/10.1086/517989)
- Woosley, S. E. 1993, ApJ, 405, 273, doi: [10.1086/172359](https://doi.org/10.1086/172359)
- Xu, F., Tang, C.-H., Geng, J.-J., et al. 2021, ApJ, 920, 135, doi: [10.3847/1538-4357/ac158a](https://doi.org/10.3847/1538-4357/ac158a)
- Xu, M., & Huang, Y. F. 2012, A&A, 538, A134, doi: [10.1051/0004-6361/201117754](https://doi.org/10.1051/0004-6361/201117754)
- Yi, S.-X., Du, M., & Liu, T. 2022, ApJ, 924, 69, doi: [10.3847/1538-4357/ac35e7](https://doi.org/10.3847/1538-4357/ac35e7)
- Yi, S.-X., Wu, X.-F., Zou, Y.-C., & Dai, Z.-G. 2020, ApJ, 895, 94, doi: [10.3847/1538-4357/ab8a53](https://doi.org/10.3847/1538-4357/ab8a53)
- Yi, S.-X., Xi, S.-Q., Yu, H., et al. 2016, ApJS, 224, 20, doi: [10.3847/0067-0049/224/2/20](https://doi.org/10.3847/0067-0049/224/2/20)
- Yonetoku, D., Murakami, T., Nakamura, T., et al. 2004, ApJ, 609, 935, doi: [10.1086/421285](https://doi.org/10.1086/421285)
- Zaninoni, E., Bernardini, M. G., Margutti, R., Oates, S., & Chincarini, G. 2013, A&A, 557, A12, doi: [10.1051/0004-6361/201321221](https://doi.org/10.1051/0004-6361/201321221)
- Zhang, B. 2006, Nature, 444, 1010, doi: [10.1038/4441010a](https://doi.org/10.1038/4441010a)
- Zhang, B., Fan, Y. Z., Dyks, J., et al. 2006, ApJ, 642, 354, doi: [10.1086/500723](https://doi.org/10.1086/500723)
- Zhang, G. Q., & Wang, F. Y. 2018, ApJ, 852, 1, doi: [10.3847/1538-4357/aa9ce5](https://doi.org/10.3847/1538-4357/aa9ce5)
- Zhao, L., Zhang, B., Gao, H., et al. 2019, ApJ, 883, 97, doi: [10.3847/1538-4357/ab38c4](https://doi.org/10.3847/1538-4357/ab38c4)
- Zitouni, H., Guessoum, N., AlQassimi, K. M., & Alaryani, O. 2018, Ap&SS, 363, 223, doi: [10.1007/s10509-018-3449-0](https://doi.org/10.1007/s10509-018-3449-0)
- Zou, L., & Liang, E.-W. 2022, MNRAS, 513, L89, doi: [10.1093/mnrasl/slac040](https://doi.org/10.1093/mnrasl/slac040)

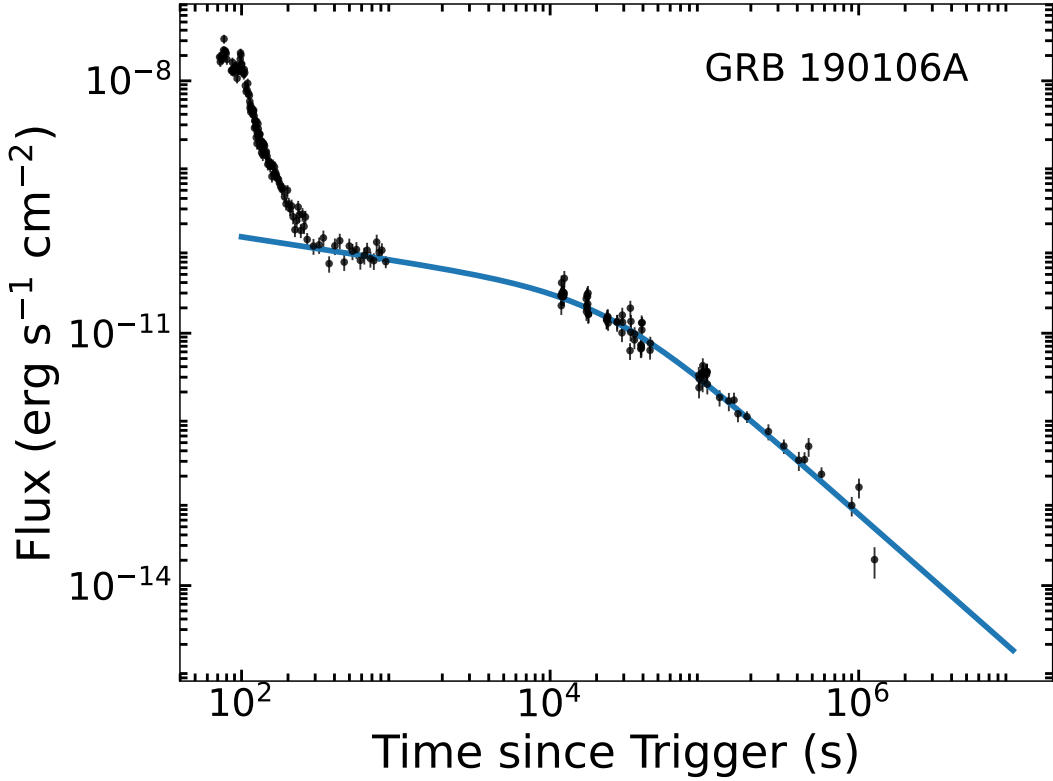


Figure 1. GRB 190106A as a typical event that has a plateau phase in the X-ray afterglow light curve. The solid curve corresponds to the best fit result by using Equation (1), through an MCMC method.

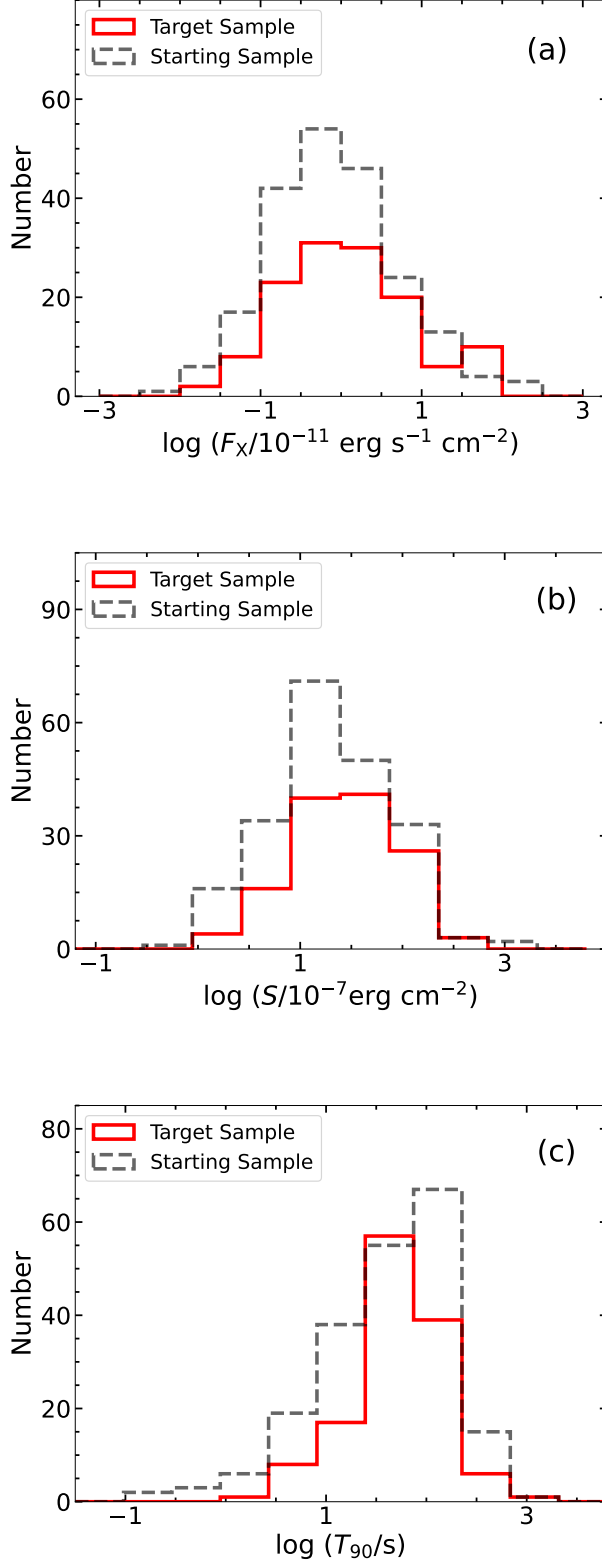


Figure 2. Distribution of F_X , S and T_{90} for the two samples. For the Starting Sample (the dashed lines), the mean values of F_X , S , and T_{90} are $0.8 \times 10^{-11} \text{ erg cm}^{-2} \text{ s}^{-1}$, $2.04 \times 10^{-6} \text{ erg cm}^{-2}$ and 39.8 s , respectively. Correspondingly, for the Target Sample (the solid lines), the mean values of F_X , S , and T_{90} are $1.2 \times 10^{-11} \text{ erg cm}^{-2} \text{ s}^{-1}$, $2.69 \times 10^{-6} \text{ erg cm}^{-2}$ and 47.9 s , respectively.

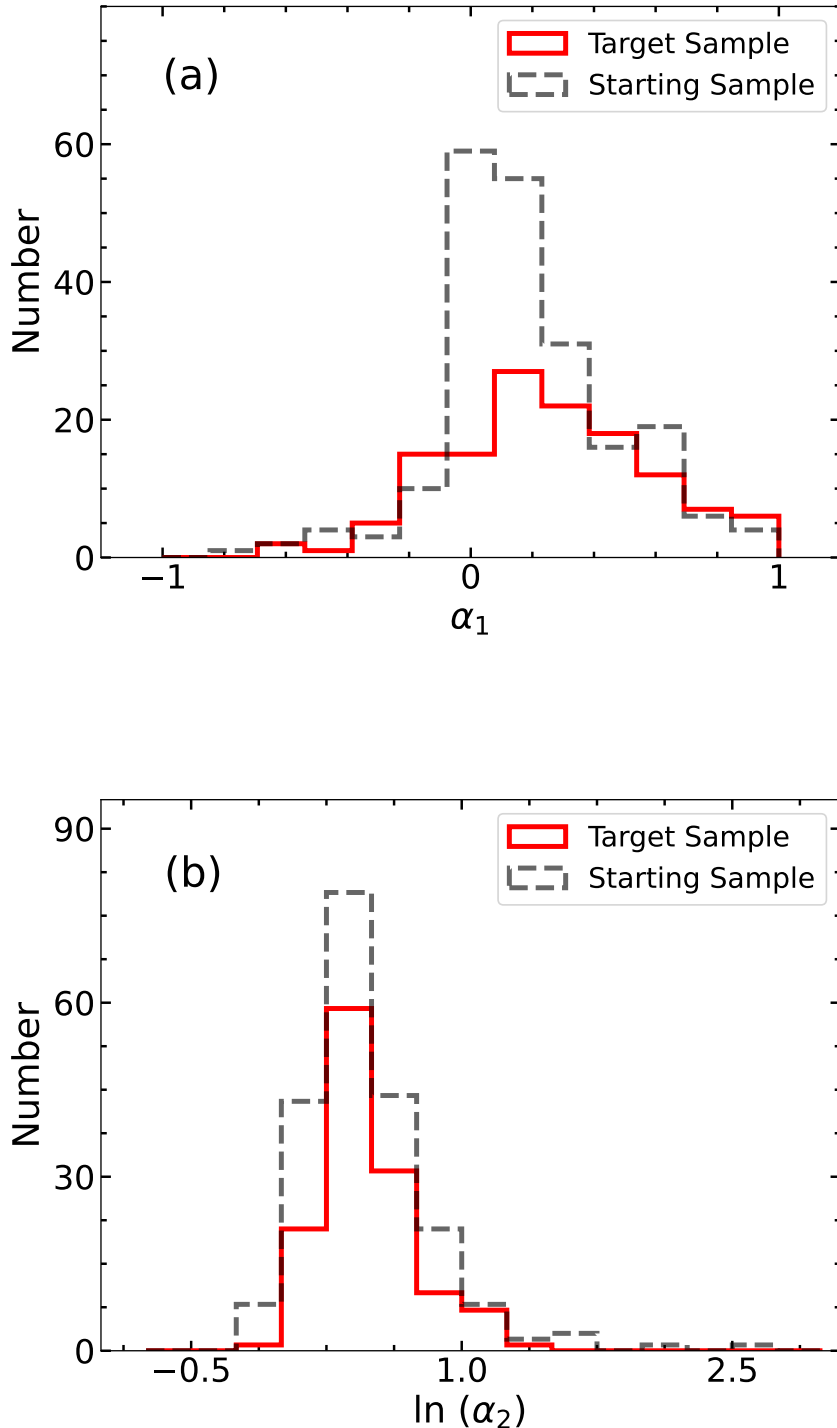


Figure 3. Distribution of the power-law index of the plateau phase (α_1) and the index after the plateau phase (α_2). The mean values of α_1 and α_2 are 0.19 and 1.77, respectively, for the Starting Sample (the dashed lines). The corresponding mean values are 0.24 and 1.68 for the Target Sample (the solid lines).

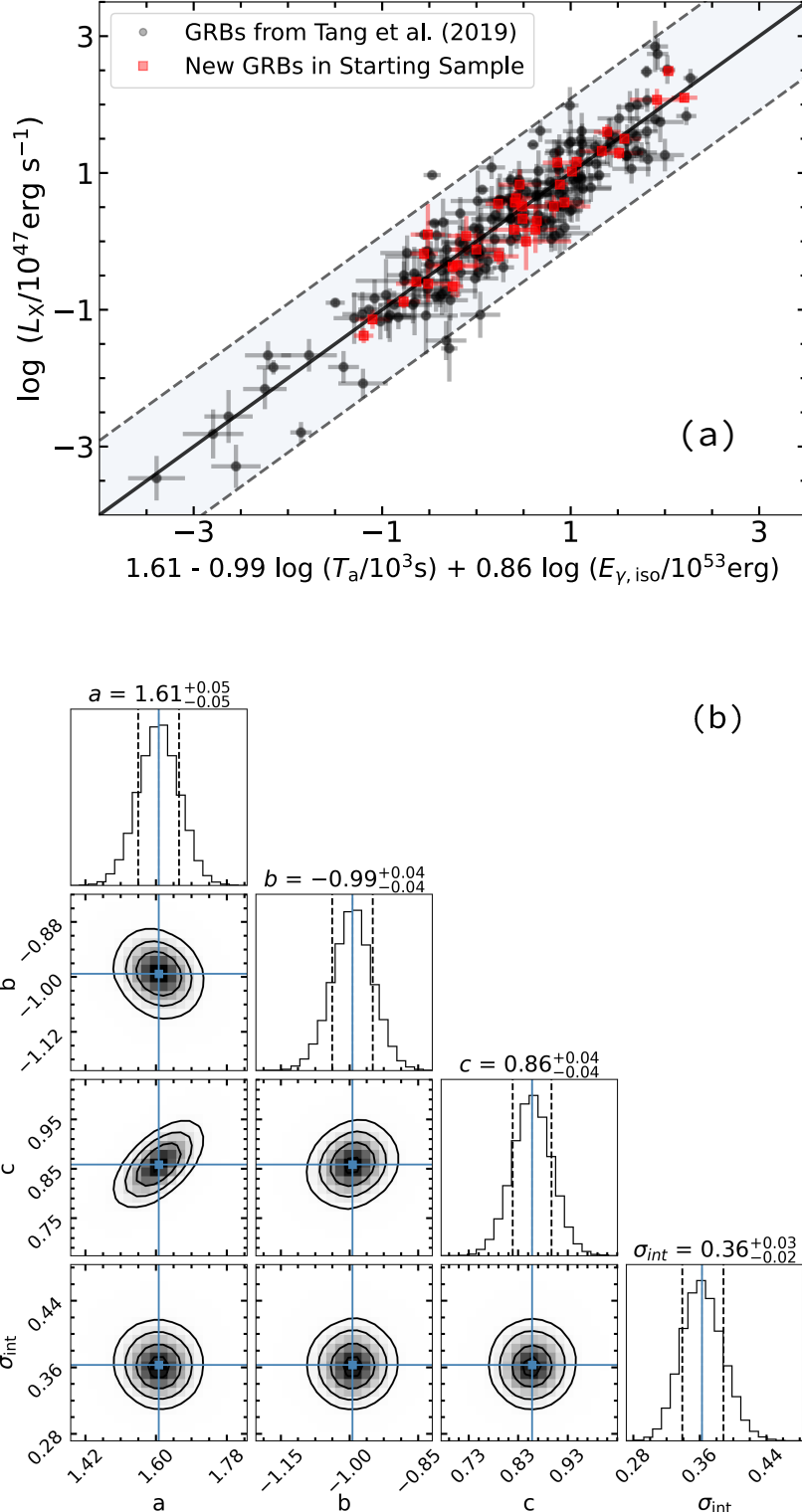


Figure 4. (a) The $L - T - E$ correlation updated with the 210 GRBs of the Starting Sample. The solid line is the best-fit result, and the dashed lines represent the 3σ confidence level. (b) Contour plots showing the uncertainty of the parameters derived from the MCMC algorithm. The vertical solid lines are the median values and the vertical dashed lines represent the 1σ confidence levels.

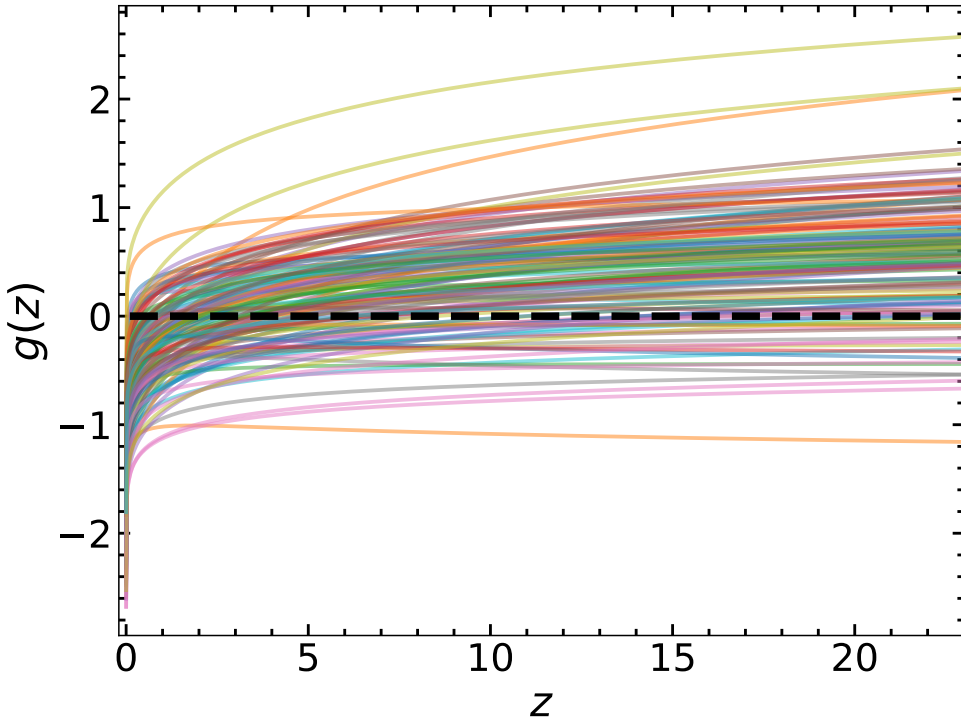


Figure 5. The function $g(z)$ as defined in Equation (10) for all the 130 GRBs in the Target Sample. The pseudo redshift of each GRB is determined by the intersection of the $g(z)$ curve with the horizontal dashed line ($g = 0$). For those GRBs whose $g(z)$ curve does not intersect with the dashed line, no pseudo redshift can be derived.

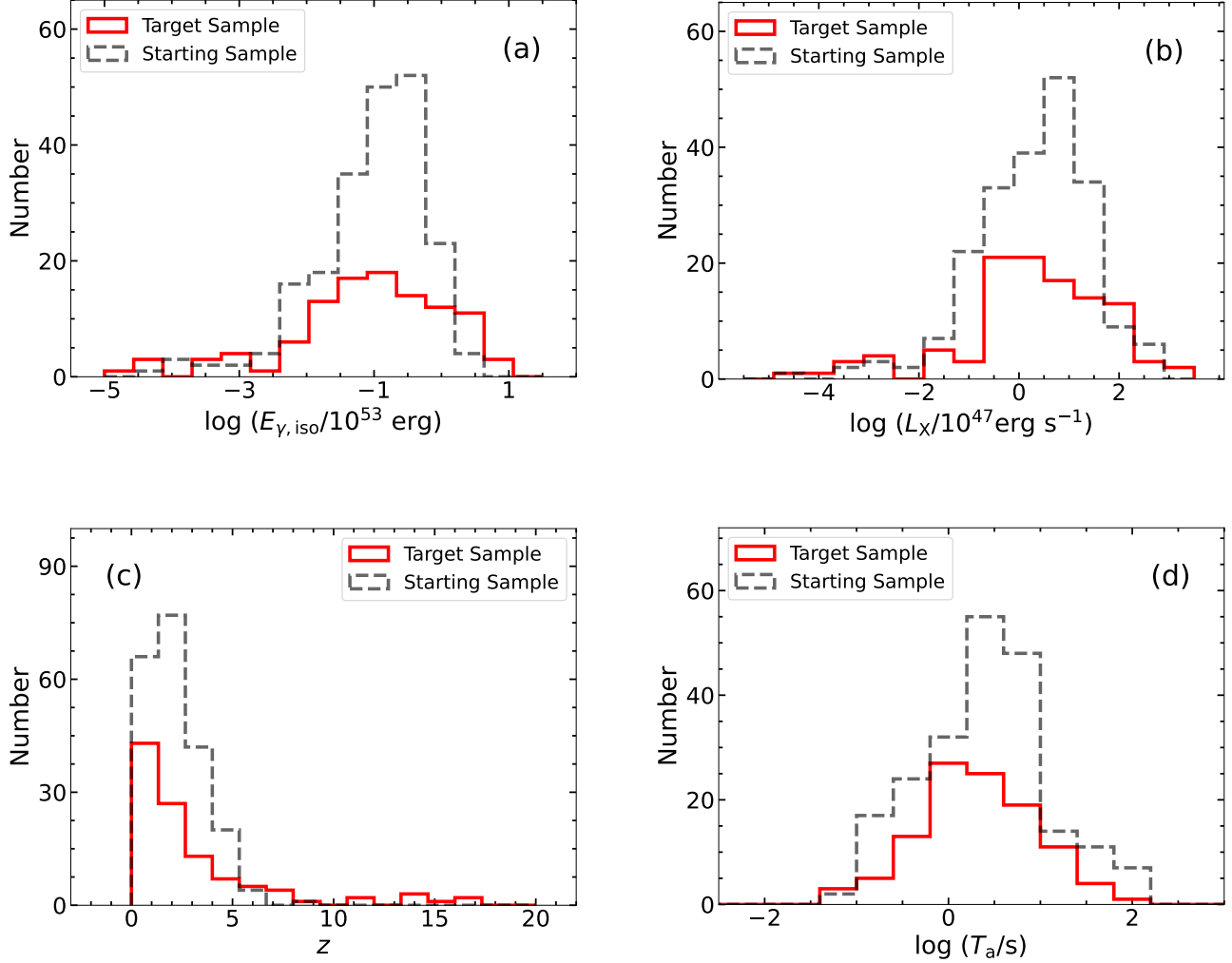


Figure 6. Distribution of $E_{\gamma, \text{iso}}$, L_X , z , and T_a for the two samples. For the Target Sample (the solid lines), the mean values of $E_{\gamma, \text{iso}}$, L_X , z and T_a are 6.46×10^{51} erg, 1.82×10^{47} erg s^{-1} , 3.08 and 2.14×10^3 s, respectively. For the Starting Sample (the dashed lines), the corresponding mean values are 8.91×10^{51} erg, 1.91×10^{47} erg s^{-1} , 2.2 and 2.51×10^3 s, respectively.

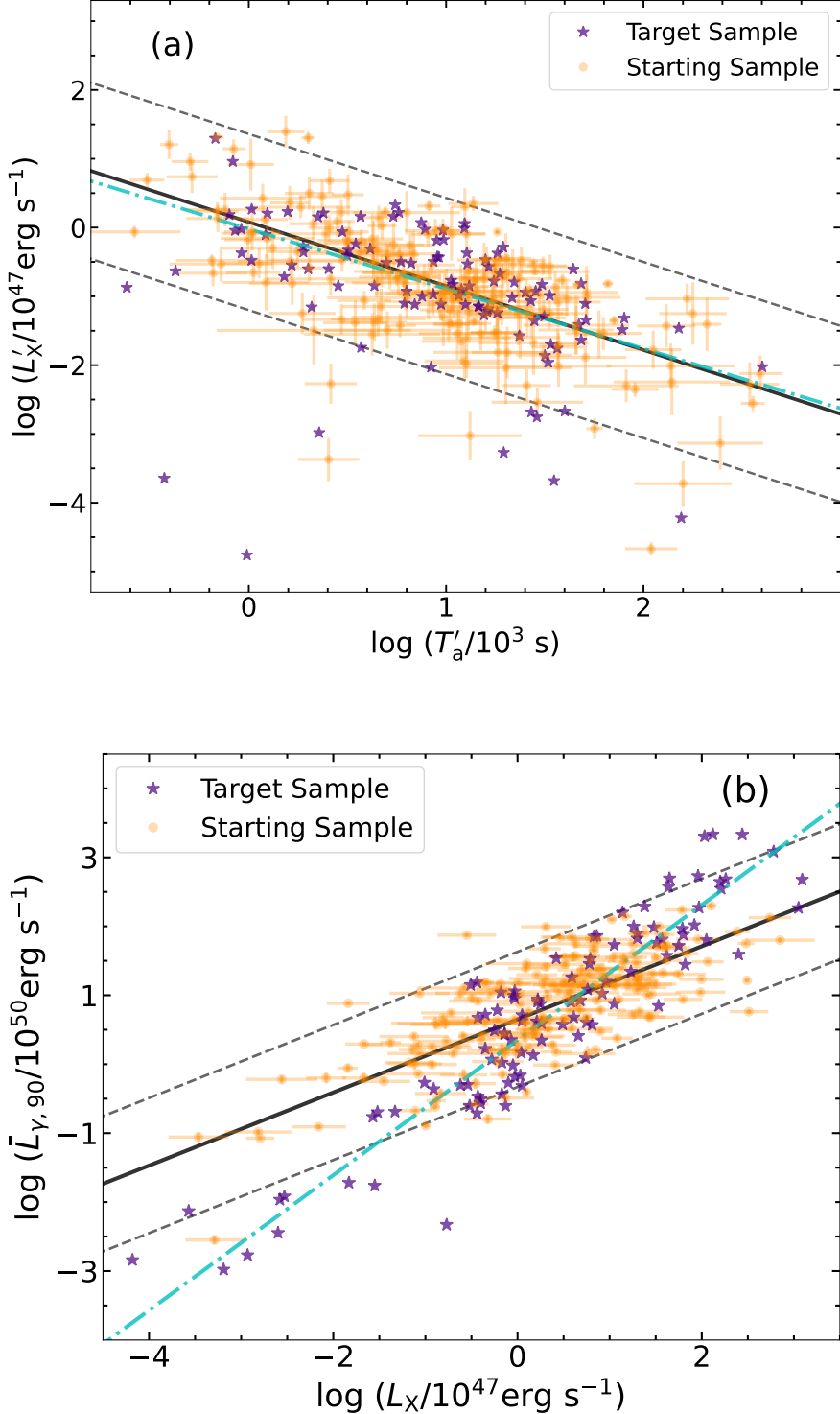


Figure 7. (a) L'_X plotted versus T'_a for the two GRB samples. The dot points correspond to the Starting Sample, which can be best fit as $L'_X \propto T_a'^{-0.93 \pm 0.08}$ (the solid line). The dashed lines correspondingly show the 2σ range. The star points correspond to the Target Sample, which mainly fall within the above 2σ range. They can be best fit as $L'_X \propto T_a'^{-0.87 \pm 0.14}$ (the dash-dotted line). Note that the two points at the lower left corner seem to be obvious outliers and are not included in the fit. (b) $\bar{L}_{\gamma,90}$ plotted versus L_X for the two GRB samples. The dot points correspond to the Starting Sample, which can be best fit as $\bar{L}_{\gamma,90} \propto L_X^{0.53 \pm 0.03}$ (the solid line). The dashed lines correspondingly show the 2σ range. The star points correspond to the Target Sample, which can be best fit as $\bar{L}_{\gamma,90} \propto L_X^{0.98 \pm 0.04}$ (the dash-dotted line). Note that the $\bar{L}_{\gamma,90} - L_X$ correlation seems to be different for the two samples.

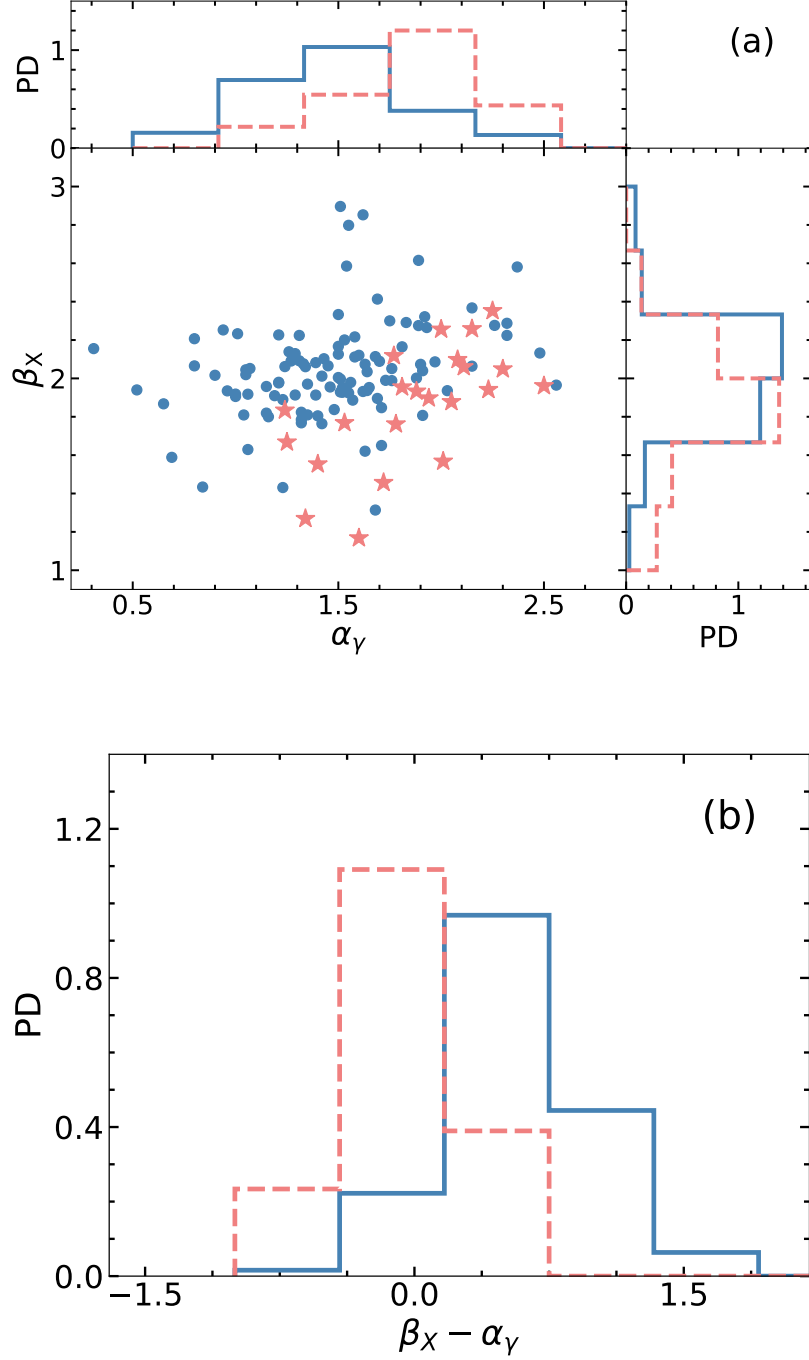


Figure 8. (a) The X-ray photon index (β_X) plotted versus the BAT γ -ray photon index (α_γ) for all the GRBs in the Target Sample. The dot points are the 108 events whose pseudo redshift can be successfully derived from the $L - T - E$ correlation, while the star symbols correspond to the remaining 22 events whose pseudo redshift cannot be calculated. The probability density (PD) distribution of these two groups are also shown. (b) The distribution of $\beta_X - \alpha_\gamma$ for the above two groups. The solid line corresponds to the 108 GRBs, while the dashed line corresponds to the remaining 22 GRBs.

Table 1. Fitting Results and Relevant Parameters of the Starting Sample. Note that only 36 GRBs are listed here, which are new events as compared with the sample of Tang et al. (2019).

| GRB Name | z | T_{90} (s) | S (15–150 keV) (10^{-7} erg cm $^{-2}$) | $\log(T_a/10^3)$ (s) | $\log(L_X/10^{47})$ (erg s $^{-1}$) | $\log(E_{\gamma,\text{iso}}/10^{53})$ (erg) | α_1 | α_2 |
|-------------|--------|-----------------|--|-------------------------|---|--|------------|------------|
| GRB 050318 | 1.44 | 32 | 10.8±0.77 | 0.63±0.18 | 0.08±0.29 | -1.27±0.03 | 0.56±0.21 | 2.21±0.18 |
| GRB 050820A | 2.612 | 26 | 34.4±2.42 | 1.55±0.17 | 0.1±0.45 | -0.68±0.03 | 0.95±0.02 | 1.51±0.05 |
| GRB 050822 | 1.434 | 103.4 | 24.6±1.72 | 0.74±0.2 | -0.22±0.12 | -0.74±0.03 | 0.14±0.09 | 1.15±0.05 |
| GRB 050915A | 2.5273 | 52 | 8.5±0.88 | 0.76±0.28 | -0.35±0.47 | -1.23±0.04 | 0.71±0.05 | 1.61±0.2 |
| GRB 050922B | 4.9 | 150.9 | 22.3±3.56 | 1.26±0.21 | 0.83±0.22 | 0.12±0.07 | -0.02±0.14 | 1.68±0.14 |
| GRB 051008 | 2.9 | 32 | 50.9±1.45 | 0.67±0.11 | 0.51±0.17 | -0.53±0.01 | 0.59±0.11 | 2.41±0.15 |
| GRB 060306 | 1.55 | 61.2 | 21.3±1.18 | -0.04±0.38 | 0.51±0.17 | -0.96±0.02 | 0.11±0.17 | 1.17±0.07 |
| GRB 060319 | 1.172 | 10.6 | 2.64±0.34 | 0.61±0.09 | -0.59±0.04 | -1.91±0.06 | -0.6±0.35 | 1.18±0.04 |
| GRB 060719 | 1.532 | 66.9 | 15±0.91 | 0.28±0.26 | 0.17±0.19 | -1.08±0.03 | 0.17±0.12 | 1.32±0.08 |
| GRB 070328 | 2.0627 | 75.3 | 90.6±1.79 | -0.77±0.04 | 2.49±0.02 | -0.39±0.01 | -0.27±0.1 | 1.53±0.02 |
| GRB 070419B | 1.9588 | 236.4 | 73.6±1.95 | 0.94±0.12 | 0.57±0.17 | -0.31±0.01 | 0.63±0.1 | 2.3±0.12 |
| GRB 070521 | 0.553 | 37.9 | 80.1±1.77 | 0.69±0.08 | -0.66±0.16 | -1.37±0.01 | 0.46±0.04 | 2.06±0.09 |
| GRB 071021 | 2.452 | 225 | 13±2 | 0.31±0.47 | 0±0.42 | -0.9±0.07 | 0.11±0.19 | 1.14±0.11 |
| GRB 080413B | 1.1 | 8 | 32±1 | 0.81±0.24 | -0.37±0.11 | -1.23±0.01 | 0.72±0.03 | 1.39±0.05 |
| GRB 080710 | 0.845 | 120 | 14±2 | 0.91±0.14 | -0.88±0.1 | -1.72±0.06 | 0.61±0.13 | 2.16±0.15 |
| GRB 081210 | 2.0631 | 146 | 18±2 | 1.95±0.06 | -1.38±0.11 | -1.01±0.05 | 0.64±0.05 | 3.71±0.54 |
| GRB 081222 | 2.7 | 24 | 48±1 | 0.66±0.17 | 0.63±0.27 | -0.62±0.01 | 0.88±0.02 | 1.65±0.07 |
| GRB 090404 | 3 | 84 | 30±1 | 0.7±0.07 | 0.83±0.06 | -0.03±0.01 | 0.12±0.05 | 1.44±0.05 |
| GRB 090426 | 2.609 | 1.2 | 1.8±0.3 | -1.28±0.23 | 1.29±0.09 | -1.59±0.07 | -0.38±0.5 | 1.09±0.06 |
| GRB 100724A | 1.288 | 1.4 | 1.6±0.2 | 0.25±0.32 | -0.62±0.27 | -2.18±0.05 | 0.69±0.09 | 1.5±0.17 |
| GRB 110801A | 1.858 | 385 | 47±3 | 0.59±0.22 | 0.17±0.34 | -0.46±0.03 | 0.7±0.09 | 1.8±0.14 |
| GRB 120907A | 0.97 | 16.9 | 6.7±1.1 | 1.13±0.14 | -1.14±0.14 | -1.85±0.07 | 0.72±0.02 | 1.39±0.08 |

Table 1 *continued on next page*

Table 1 (*continued*)

| GRB Name | z | T_{90} (s) | S (15-150 keV) (10^{-7} erg cm $^{-2}$) | $\log (T_a/10^3)$ (s) | $\log (L_x/10^{47})$ (erg s $^{-1}$) | $\log (E_{\gamma, \text{iso}}/10^{53})$ (erg) | α_1 | α_2 |
|-------------|--------|-----------------|--|--------------------------|--|--|------------------|-----------------|
| GRB 130505A | 2.27 | 88 | 210 \pm 10 | 0.49 \pm 0.13 | 1.6 \pm 0.11 | 0.31 \pm 0.02 | 0.39 \pm 0.13 | 1.63 \pm 0.04 |
| GRB 130609B | 1.3 | 210.6 | 160 \pm 0 | 0.79 \pm 0.05 | 0.33 \pm 0.08 | -0.39 \pm 0 | 0.85 \pm 0.03 | 2.84 \pm 0.14 |
| GRB 140419A | 3.956 | 94.7 | 160 \pm 0 | -0.18 \pm 0.28 | 2.07 \pm 0.16 | 0.15 \pm 0 | 0.3 \pm 0.19 | 1.48 \pm 0.07 |
| GRB 150314A | 1.758 | 14.79 | 220 \pm 3 | 0.45 \pm 0.07 | 1.02 \pm 0.05 | -0.17 \pm 0.01 | -0.41 \pm 0.3 | 1.95 \pm 0.07 |
| GRB 161014A | 2.823 | 18.3 | 19 \pm 2 | 0.09 \pm 0.13 | 1.15 \pm 0.2 | -0.77 \pm 0.05 | 0.55 \pm 0.08 | 2.52 \pm 0.18 |
| GRB 190106A | 1.86 | 76.8 | 60 \pm 2 | 0.92 \pm 0.12 | 0.55 \pm 0.13 | -0.54 \pm 0.01 | 0.28 \pm 0.05 | 1.62 \pm 0.06 |
| GRB 190114A | 3.3765 | 66.6 | 8 \pm 1.2 | -0.3 \pm 0.22 | 1.32 \pm 0.09 | -0.67 \pm 0.07 | -0.09 \pm 0.19 | 1.25 \pm 0.1 |
| GRB 191011A | 1.722 | 7.37 | 3.3 \pm 0.4 | -0.73 \pm 0.18 | 0.57 \pm 0.09 | -1.63 \pm 0.05 | -0.24 \pm 0.24 | 1.36 \pm 0.09 |
| GRB 200829A | 1.25 | 13.04 | 510 \pm 10 | 0.47 \pm 0.06 | 1.16 \pm 0.08 | -0.09 \pm 0.01 | 0.87 \pm 0.01 | 1.89 \pm 0.04 |
| GRB 201221A | 5.7 | 44.5 | 18 \pm 2 | 0.54 \pm 0.1 | 0.3 \pm 0.17 | -0.5 \pm 0.05 | 0.585 \pm 0.05 | 2.92 \pm 0.75 |
| GRB 210210A | 0.715 | 6.6 | 9.8 \pm 0.8 | 0.46 \pm 0.1 | -0.18 \pm 0.1 | -1.99 \pm 0.04 | 0.29 \pm 0.07 | 1.8 \pm 0.11 |
| GRB 210610A | 3.54 | 13.62 | 10 \pm 1 | -0.8 \pm 0.16 | 1.5 \pm 0.06 | -0.97 \pm 0.04 | -0.39 \pm 0.18 | 1.12 \pm 0.07 |
| GRB 210722A | 1.145 | 50.2 | 25 \pm 2 | 0.59 \pm 0.28 | -0.12 \pm 0.32 | -1.19 \pm 0.03 | 0.63 \pm 0.09 | 1.73 \pm 0.17 |
| GRB 220521A | 5.6 | 13.55 | 8.1 \pm 0.8 | -0.94 \pm 0.12 | 2.1 \pm 0.06 | -0.39 \pm 0.04 | -0.56 \pm 0.21 | 1.68 \pm 0.14 |

Table 2. Fitting Results and Relevant Parameters of 130 GRBs in the Target Sample

| GRB Name | z_{est} | T_{90} (s) | $\log F_X$ (erg cm $^{-2}$ s $^{-1}$) | S (15–150 keV) (10 $^{-7}$ erg cm $^{-2}$) | $\log (T_a/10^3)$ (s) | $\log (L_X/10^{47})$ (erg s $^{-1}$) | $\log (E_{\gamma,\text{iso}}/10^{53})$ | α_1 | α_2 |
|-------------|------------------|-----------------|---|--|--------------------------|--|--|------------|------------|
| GRB 050607 | 14.21 | 26.4 | -11.89±0.24 | 5.92±0.55 | -0.4±0.46 | 1.96±0.24 | -0.03±0.04 | 0.21±0.19 | 1.3±0.14 |
| GRB 050712 | 2.4 | 51.6 | -12.08±0.17 | 10.8±1.19 | 1.02±0.18 | -0.35±0.17 | -1.1±0.05 | 0.46±0.08 | 1.3±0.07 |
| GRB 050713A | 2.54 | 124.7 | -11.08±0.22 | 51.1±2.12 | 0.53±0.17 | 0.76±0.22 | -0.37±0.02 | 0.53±0.04 | 1.43±0.05 |
| GRB 050713B | 0.32 | 54.2 | -11.12±0.13 | 31.8±3.18 | 1.35±0.1 | -1.57±0.13 | -2.15±0.04 | 0.16±0.07 | 1.36±0.05 |
| GRB 050726 | 1.05 | 49.9 | -10.95±0.35 | 19.4±2.12 | 0.41±0.22 | -0.17±0.35 | -1.59±0.05 | 0.66±0.1 | 2.01±0.17 |
| GRB 060105 | 0.67 | 54.4 | -9.57±0.04 | 176±3.04 | 0.1±0.04 | 0.75±0.04 | -0.88±0.01 | 0.68±0.02 | 2±0.06 |
| GRB 060109 | 0.98 | 115.4 | -11.18±0.08 | 6.55±1.03 | 0.47±0.1 | -0.4±0.08 | -1.8±0.07 | -0.21±0.11 | 1.68±0.1 |
| GRB 060111B | 2.55 | 58.8 | -11.65±0.47 | 16±1.42 | 0.41±0.27 | 0.21±0.47 | -1.16±0.04 | 0.7±0.08 | 1.74±0.18 |
| GRB 060204B | 1.44 | 139.4 | -11.25±0.32 | 29.5±1.78 | 0.58±0.25 | -0.05±0.32 | -1.26±0.03 | 0.6±0.08 | 1.71±0.11 |
| GRB 060413 | 0.08 | 147.7 | -10.76±0.04 | 35.6±1.47 | 1.39±0.03 | -2.6±0.04 | -3.31±0.02 | -0.13±0.09 | 3.43±0.17 |
| GRB 060428A | 0.04 | 39.5 | -11.79±0.08 | 13.9±0.78 | 2.17±0.07 | -4.18±0.08 | -4.26±0.02 | 0.48±0.02 | 1.68±0.06 |
| GRB 060510A | 0.2 | 20.4 | -9.97±0.06 | 80.5±3.12 | 0.69±0.06 | -0.91±0.06 | -2.13±0.02 | 0.05±0.05 | 1.55±0.03 |
| GRB 060712 | 3.65 | 26.3 | -11.89±0.27 | 12.4±2.17 | 0.2±0.42 | 0.79±0.27 | -0.72±0.08 | 0.12±0.16 | 1.24±0.12 |
| GRB 060807 | 0.21 | 54 | -10.96±0.05 | 8.48±1.09 | 0.82±0.06 | -1.83±0.05 | -3.07±0.06 | -0.1±0.06 | 1.85±0.06 |
| GRB 060813 | 0.98 | 16.1 | -10.45±0.11 | 54.6±1.4 | 0.4±0.15 | 0.22±0.11 | -1.15±0.01 | 0.61±0.04 | 1.62±0.06 |
| GRB 061202 | 0.42 | 91.2 | -11.16±0.05 | 34.2±1.33 | 1.34±0.05 | -1.33±0.05 | -1.88±0.02 | 0.12±0.05 | 2.33±0.11 |
| GRB 070107 | 4.78 | 347.3 | -12.62±0.07 | 51.7±2.64 | 1.65±0.04 | -0.18±0.07 | -0.18±0.02 | 0.9±0.01 | 2.84±0.3 |
| GRB 070420 | 3.31 | 76.5 | -10.47±0.1 | 140±4.48 | 0.1±0.11 | 1.51±0.1 | 0.01±0.01 | 0.27±0.08 | 1.66±0.05 |
| GRB 070628 | 0.82 | 39.1 | -10.66±0.1 | 35±2 | 0.7±0.11 | -0.14±0.1 | -1.22±0.02 | 0.22±0.06 | 1.51±0.08 |
| GRB 071118 | 0.08 | 71 | -11.36±0.09 | 5±1 | 1.25±0.05 | -3.19±0.09 | -4.16±0.09 | 0.61±0.05 | 4±1.05 |
| GRB 080212 | 0.92 | 123 | -11.11±0.23 | 29±3 | 0.62±0.38 | -0.43±0.23 | -1.66±0.04 | 0.3±0.28 | 1.63±0.16 |
| GRB 080229A | 0.34 | 64 | -9.66±0.11 | 90±2 | 0.34±0.15 | -0.1±0.11 | -1.59±0.01 | 0.18±0.12 | 1.36±0.03 |
| GRB 080328 | 6.3 | 90.6 | -9.57±0.07 | 94±2 | -1.16±0.27 | 3.05±0.07 | 0.36±0.01 | -0.16±0.4 | 1.19±0.07 |

Table 2 continued on next page

Table 2 (*continued*)

| GRB Name | z_{est} | T_{90} (s) | $\log F_X$ (erg cm $^{-2}$ s $^{-1}$) | S (15–150 keV) (10 $^{-7}$ erg cm $^{-2}$) | $\log (T_{\text{a}}/10^3)$ (s) | $\log (L_X/10^{47})$ (erg s $^{-1}$) | $\log (E_{\gamma,\text{iso}}/10^{53})$ (erg) | α_1 | α_2 |
|-------------|------------------|-----------------|---|--|-----------------------------------|--|---|------------|------------|
| GRB 080903 | 0.1 | 66 | -9.14±0.06 | 14±1 | -0.67±0.06 | -0.77±0.06 | -3.55±0.03 | -0.03±0.14 | 2.06±0.05 |
| GRB 081230 | 16.32 | 60.7 | -12.06±0.36 | 8.2±0.8 | 0.16±0.25 | 1.65±0.36 | 0.24±0.04 | 0.47±0.06 | 1.46±0.15 |
| GRB 090111 | 14.16 | 24.8 | -12.12±0.49 | 6.2±0.6 | 0.01±0.4 | 2.03±0.49 | 0.52±0.04 | 0.24±0.19 | 1.3±0.5 |
| GRB 090518 | 1.35 | 6.9 | -11.21±0.26 | 4.7±0.4 | -0.01±0.54 | 0.05±0.26 | -1.82±0.04 | 0.19±0.17 | 1.18±0.15 |
| GRB 090813 | 0.2 | 7.1 | -9.49±0.03 | 13±1 | -0.47±0.06 | -0.44±0.03 | -2.94±0.03 | -0.14±0.08 | 1.32±0.02 |
| GRB 091130B | 2.33 | 112.5 | -12.05±0.12 | 13±1 | 1.24±0.17 | -0.22±0.12 | -0.69±0.03 | 0.13±0.09 | 1.4±0.11 |
| GRB 100305A | 1.78 | 69.7 | -11.46±0.16 | 15±2 | 0.61±0.16 | -0.07±0.16 | -1.25±0.06 | 0.11±0.28 | 2.32±0.31 |
| GRB 100508A | 0.18 | 52 | -11.51±0.05 | 7±1.1 | 1.37±0.04 | -2.58±0.05 | -3.32±0.07 | 0.33±0.04 | 3.29±0.3 |
| GRB 100522A | 1.65 | 35.3 | -11.42±0.21 | 21±1 | 0.9±0.21 | -0.04±0.21 | -0.88±0.02 | 0.4±0.06 | 1.43±0.12 |
| GRB 100619A | 7.08 | 97.5 | -11.67±0.3 | 45±1 | 0.55±0.2 | 1.38±0.3 | 0.37±0.01 | 0.69±0.03 | 1.34±0.09 |
| GRB 100725B | 5.13 | 200 | -11.64±0.17 | 68±2 | 0.66±0.14 | 1.3±0.17 | 0.41±0.01 | 0.43±0.06 | 1.73±0.15 |
| GRB 100727A | 2.89 | 84 | -11.38±0.06 | 12±1 | 0.38±0.18 | 0.58±0.06 | -0.76±0.04 | -0.2±0.11 | 1.09±0.11 |
| GRB 101023A | 7.2 | 80.8 | -10.73±0.2 | 270±10 | -0.05±0.26 | 2.2±0.2 | 0.64±0.02 | 0.44±0.2 | 1.59±0.08 |
| GRB 101024A | 1.25 | 18.7 | -10.09±0.06 | 15±1 | -0.51±0.09 | 0.81±0.06 | -1.51±0.03 | -0.37±0.18 | 1.37±0.05 |
| GRB 101117B | 4.46 | 5.2 | -10.47±0.08 | 11±1 | -1.02±0.13 | 1.97±0.08 | -0.75±0.04 | -0.5±0.47 | 1.28±0.07 |
| GRB 110102A | 4 | 264 | -10.53±0.08 | 165±3 | 0.22±0.09 | 1.75±0.08 | 0.44±0.01 | 0.24±0.05 | 1.48±0.04 |
| GRB 110106B | 3.63 | 24.8 | -11.31±0.24 | 20±1 | 0.41±0.17 | 0.83±0.24 | -0.42±0.02 | 0.47±0.06 | 1.51±0.08 |
| GRB 110210A | 5.51 | 233 | -11.84±0.08 | 9.6±1.9 | 0.48±0.37 | 0.68±0.08 | -0.52±0.09 | -0.23±0.22 | 0.93±0.14 |
| GRB 110223A | 0.11 | 7 | -12.1±0.17 | 1.6±0.4 | 1.49±0.14 | -3.57±0.17 | -4.33±0.11 | 0.34±0.05 | 1.05±0.07 |
| GRB 110312A | 1.41 | 28.7 | -11.61±0.13 | 8.2±1.3 | 0.97±0.1 | -0.43±0.13 | -1.25±0.07 | 0.32±0.05 | 1.17±0.07 |
| GRB 110319A | 1.88 | 19.3 | -11.54±0.34 | 14±1 | 0.59±0.28 | -0.03±0.34 | -1.22±0.03 | 0.52±0.07 | 1.57±0.15 |
| GRB 110411A | 3.88 | 80.3 | -10.97±0.21 | 33±2 | -0.51±0.52 | 1.82±0.21 | -0.34±0.03 | 0.04±0.25 | 1.26±0.18 |
| GRB 110709A | 1.99 | 44.7 | -10.72±0.03 | 100±2 | 0.51±0.01 | 0.78±0.03 | -0.37±0.01 | 0.67±0.01 | 2.85±0.16 |
| GRB 110709B | 1.65 | 55.6 | -11.76±0.15 | 94±2 | 1.65±0.1 | -0.44±0.15 | -0.49±0.01 | 0.87±0.03 | 2±0.1 |
| GRB 110915A | 1.1 | 78.76 | -10.64±0.26 | 57±2 | 0.42±0.22 | 0.26±0.26 | -1.08±0.02 | 0.78±0.04 | 1.47±0.07 |

Table 2 (*continued on next page*)

Table 2 (*continued*)

| GRB Name | z_{est} | T_{90} (s) | $\log F_X$ (erg cm $^{-2}$ s $^{-1}$) | S (15–150 keV) (10 $^{-7}$ erg cm $^{-2}$) | $\log (T_{\text{a}}/10^3)$ (s) | $\log (L_X/10^{47})$ (erg s $^{-1}$) | $\log (E_{\gamma,\text{iso}}/10^{53})$ (erg) | α_1 | α_2 |
|-------------|------------------|-----------------|---|--|-----------------------------------|--|---|------------|------------|
| GRB 111129A | 0.05 | 7.6 | -10.77±0.2 | 1.8±0.4 | 0.33±0.25 | -2.93±0.2 | -4.91±0.1 | 0.27±0.1 | 1.32±0.07 |
| GRB 120116A | 5.95 | 41 | -10.89±0.16 | 29±1 | -0.51±0.45 | 1.8±0.16 | -0.35±0.01 | -0.11±0.23 | 1.1±0.14 |
| GRB 120308A | 1.33 | 60.6 | -11.26±0.11 | 12±1 | 0.8±0.07 | -0.35±0.11 | -1.36±0.04 | 0.56±0.04 | 2.61±0.2 |
| GRB 120324A | 1.87 | 118 | -10.51±0.13 | 101±3 | 0.38±0.16 | 0.92±0.13 | -0.36±0.01 | 0.2±0.07 | 1.4±0.08 |
| GRB 120701A | 3.99 | 13.8 | -11.81±0.35 | 14±1 | 0.32±0.14 | 0.42±0.35 | -1.02±0.03 | 0.85±0.04 | 1.76±0.18 |
| GRB 120703A | 4 | 25.2 | -10.94±0.36 | 35±1 | 0.09±0.33 | 1.26±0.36 | -0.3±0.01 | 0.5±0.06 | 1.31±0.07 |
| GRB 121031A | 0.96 | 226 | -11.06±0.38 | 78±2 | 1.16±0.22 | -0.28±0.38 | -0.87±0.01 | 0.39±0.08 | 1.55±0.34 |
| GRB 121123A | 7.83 | 317 | -11.2±0.06 | 150±10 | 0.09±0.17 | 1.62±0.06 | 0.13±0.03 | -0.35±0.3 | 1.49±0.15 |
| GRB 121217A | 1.23 | 778 | -10.89±0.08 | 62±3 | 0.91±0.11 | 0.05±0.08 | -0.77±0.02 | 0.12±0.08 | 1.52±0.07 |
| GRB 130327A | 2.27 | 9 | -12.26±0.16 | 2.3±0.5 | 0.92±0.14 | -0.51±0.16 | -1.41±0.09 | 0.05±0.06 | 1.36±0.5 |
| GRB 130504A | 0.2 | 50 | -10.6±0.22 | 10±1 | 0.47±0.23 | -1.55±0.22 | -3.14±0.04 | 0.27±0.16 | 1.78±0.22 |
| GRB 130528A | 14.18 | 59.4 | -10.27±0.12 | 51±2 | -1.28±0.21 | 3.09±0.12 | 0.27±0.02 | -0.14±0.25 | 1.13±0.04 |
| GRB 130803A | 3.33 | 44 | -11.05±0.43 | 15±1 | -0.18±0.6 | 1.23±0.43 | -0.65±0.03 | 0.44±0.11 | 1.03±0.1 |
| GRB 131002A | 3.38 | 55.59 | -10.54±0.14 | 6.4±0.8 | -0.84±0.52 | 1.53±0.14 | -1.05±0.05 | -0.05±0.34 | 1.11±0.1 |
| GRB 140108A | 1.12 | 94 | -10.57±0.18 | 70±2 | 0.7±0.19 | 0.26±0.18 | -0.76±0.01 | 0.36±0.1 | 1.64±0.15 |
| GRB 140323A | 3.52 | 104.9 | -10.74±0.27 | 160±0 | 0.47±0.2 | 1.3±0.27 | 0.19±0 | 0.54±0.09 | 2±0.22 |
| GRB 140709A | 1.57 | 98.6 | -11.12±0.23 | 53±2 | 0.89±0.22 | 0.05±0.23 | -0.79±0.02 | 0.44±0.08 | 1.59±0.15 |
| GRB 140817A | 8.51 | 244 | -11.76±0.27 | 46±2 | 0.68±0.12 | 1.05±0.27 | 0.14±0.02 | 0.71±0.1 | 2.65±0.39 |
| GRB 140916A | 0.14 | 80.1 | -11.28±0.05 | 17±3 | 1.53±0.06 | -2.53±0.05 | -3.07±0.08 | -0.2±0.08 | 2.3±0.18 |
| GRB 141017A | 1.59 | 55.7 | -10.74±0.19 | 31±1 | 0.18±0.29 | 0.49±0.19 | -1.09±0.01 | 0.16±0.12 | 1.34±0.11 |
| GRB 150201A | 0.004 | 26.1 | -9.13±0.03 | 7.8±1.2 | -0.43±0.07 | -3.64±0.03 | -6.63±0.07 | -0.15±0.12 | 1.3±0.02 |
| GRB 150202A | 2.16 | 25.7 | -10.95±0.29 | 6.1±0.7 | -0.22±0.24 | 0.61±0.29 | -1.41±0.05 | 0.46±0.1 | 1.64±0.22 |
| GRB 150203A | 6.79 | 25.8 | -11.66±0.28 | 9.1±0.6 | 0.22±0.18 | 1.14±0.28 | -0.28±0.03 | 0.19±0.15 | 2.47±0.9 |
| GRB 150428B | 3.72 | 130.9 | -11.84±0.2 | 37±3 | 0.83±0.17 | 0.22±0.2 | -0.65±0.04 | 0.09±0.08 | 1.27±0.15 |
| GRB 150430A | 5.04 | 107.1 | -10.47±0.13 | 69±5 | -0.41±0.15 | 2.05±0.13 | 0.05±0.03 | 0.17±0.18 | 1.97±0.14 |

Table 2 *continued on next page*

Table 2 (*continued*)

| GRB Name | z_{est} | T_{90} (s) | $\log F_X$ (erg cm $^{-2}$ s $^{-1}$) | S (15–150 keV) (10 $^{-7}$ erg cm $^{-2}$) | $\log (T_{\text{a}}/10^3)$ (s) | $\log (L_X/10^{47})$ (erg s $^{-1}$) | $\log (E_{\gamma,\text{iso}}/10^{53})$ (erg) | α_1 | α_2 |
|-------------|------------------|-----------------|---|--|-----------------------------------|--|---|------------------|-----------------|
| GRB 160119A | 11.25 | 116 | -11.11 \pm 0.09 | 71 \pm 2 | -0.1 \pm 0.29 | 2.26 \pm 0.09 | 0.66 \pm 0.01 | -0.2 \pm 0.36 | 1.45 \pm 0.21 |
| GRB 160504A | 1.79 | 53.9 | -11.49 \pm 0.13 | 7.3 \pm 0.9 | 0.65 \pm 0.16 | -0.14 \pm 0.13 | -1.28 \pm 0.05 | 0.08 \pm 0.07 | 1.52 \pm 0.18 |
| GRB 160607A | 2.32 | 33.4 | -10.12 \pm 0.13 | 210 \pm 0 | 0.11 \pm 0.12 | 1.48 \pm 0.13 | -0.01 \pm 0 | 0.62 \pm 0.035 | 1.52 \pm 0.04 |
| GRB 160630A | 0.73 | 29.5 | -10.31 \pm 0.09 | 12 \pm 1 | -0.08 \pm 0.16 | 0.03 \pm 0.09 | -1.93 \pm 0.04 | -0.03 \pm 0.12 | 1.25 \pm 0.07 |
| GRB 160824A | 0.71 | 99.3 | -10.97 \pm 0.16 | 26 \pm 2 | 0.92 \pm 0.09 | -0.62 \pm 0.16 | -1.54 \pm 0.03 | 0.39 \pm 0.05 | 2.17 \pm 0.32 |
| GRB 160905A | 0.33 | 64 | -9.57 \pm 0.06 | 150 \pm 2 | 0.35 \pm 0.06 | -0.03 \pm 0.06 | -1.5 \pm 0.01 | 0.64 \pm 0.02 | 1.58 \pm 0.03 |
| GRB 161004B | 15.33 | 15.9 | -11.08 \pm 0.37 | 88 \pm 2 | -0.58 \pm 0.28 | 2.44 \pm 0.37 | 0.32 \pm 0.01 | 0.76 \pm 0.06 | 1.73 \pm 0.18 |
| GRB 161202A | 3.09 | ... | -11.26 \pm 0.59 | 86 \pm 3 | 0.43 \pm 0.38 | 1.16 \pm 0.59 | -0.02 \pm 0.02 | 0.7 \pm 0.08 | 1.72 \pm 0.24 |
| GRB 161214B | 17.15 | 24.8 | -11.52 \pm 0.13 | 24 \pm 1 | -0.12 \pm 0.48 | 2.12 \pm 0.13 | 0.47 \pm 0.02 | -0.15 \pm 0.39 | 1.32 \pm 0.17 |
| GRB 170317A | 1.84 | 11.94 | -11.16 \pm 0.23 | 13 \pm 1 | 0.07 \pm 0.24 | 0.25 \pm 0.23 | -1.5 \pm 0.03 | 0.39 \pm 0.09 | 1.66 \pm 0.2 |
| GRB 170803A | 0.001 | 3.82 | -9.33 \pm 0.02 | 9.8 \pm 0.4 | -0.01 \pm 0.05 | -4.76 \pm 0.02 | -7.44 \pm 0.02 | 0.15 \pm 0.07 | 1.97 \pm 0.05 |
| GRB 170906A | 1.86 | 88.1 | -9.1 \pm 0.03 | 320 \pm 0 | -0.74 \pm 0.08 | 2.4 \pm 0.03 | 0.08 \pm 0 | -0.58 \pm 0.29 | 1.76 \pm 0.05 |
| GRB 171120A | 1.78 | 64 | -11.34 \pm 0.11 | 86 \pm 3 | 1.15 \pm 0.08 | -0.03 \pm 0.11 | -0.58 \pm 0.02 | 0.21 \pm 0.06 | 1.98 \pm 0.16 |
| GRB 180411A | 3.16 | 77.5 | -10.36 \pm 0.14 | 120 \pm 0 | 0.11 \pm 0.15 | 1.57 \pm 0.14 | 0.08 \pm 0 | 0.08 \pm 0.1 | 1.45 \pm 0.09 |
| GRB 180623A | 4.69 | 114.9 | -10.62 \pm 0.2 | 120 \pm 2 | 0.04 \pm 0.1 | 1.79 \pm 0.2 | 0.27 \pm 0.01 | 0.46 \pm 0.08 | 2.59 \pm 0.23 |
| GRB 180626A | 6.44 | 30.07 | -11.07 \pm 0.15 | 48 \pm 2 | 0.11 \pm 0.17 | 1.64 \pm 0.15 | 0.18 \pm 0.02 | 0.24 \pm 0.06 | 1.44 \pm 0.1 |
| GRB 190202A | 0.21 | 19.4 | -9.29 \pm 0.05 | 60 \pm 5 | -0.14 \pm 0.05 | -0.17 \pm 0.05 | -2.23 \pm 0.04 | -0.01 \pm 0.06 | 1.5 \pm 0.02 |
| GRB 190203A | 1.95 | 96 | -10.31 \pm 0.12 | 150 \pm 5 | 0.4 \pm 0.07 | 0.96 \pm 0.12 | -0.29 \pm 0.01 | 0.9 \pm 0.02 | 2.11 \pm 0.1 |
| GRB 190211A | 0.85 | 12.48 | -10.36 \pm 0.06 | 6.5 \pm 1.2 | -0.32 \pm 0.13 | 0.17 \pm 0.06 | -2.04 \pm 0.08 | -0.33 \pm 0.2 | 1.29 \pm 0.06 |
| GRB 190519A | 11.08 | 45.58 | -10.2 \pm 0.17 | 180 \pm 10 | -0.62 \pm 0.21 | 2.78 \pm 0.17 | 0.66 \pm 0.02 | 0.23 \pm 0.09 | 1.41 \pm 0.1 |
| GRB 190828B | 1.88 | 66.6 | -10.32 \pm 0.14 | 42 \pm 2 | -0.1 \pm 0.04 | 1.05 \pm 0.14 | -0.76 \pm 0.02 | -0.03 \pm 0.05 | 1.39 \pm 0.04 |
| GRB 191004A | 1.94 | 2.44 | -10.49 \pm 0.14 | 13 \pm 1 | -0.31 \pm 0.14 | 0.86 \pm 0.14 | -1.22 \pm 0.03 | 0.54 \pm 0.06 | 1.8 \pm 0.12 |
| GRB 200519A | 0.24 | 71.88 | -9.34 \pm 0.03 | 120 \pm 2 | 0.16 \pm 0.05 | -0.13 \pm 0.03 | -1.84 \pm 0.01 | 0.28 \pm 0.03 | 1.41 \pm 0.02 |
| GRB 200711A | 1.63 | 29.39 | -10.66 \pm 0.24 | 53 \pm 3 | 0.43 \pm 0.19 | 0.59 \pm 0.24 | -0.69 \pm 0.02 | 0.47 \pm 0.07 | 1.85 \pm 0.19 |
| GRB 200713A | 0.71 | 48.98 | -11.4 \pm 0.15 | 9 \pm 1.6 | 1.08 \pm 0.18 | -1.01 \pm 0.15 | -1.81 \pm 0.08 | 0.11 \pm 0.09 | 1.51 \pm 0.18 |

Table 2 *continued on next page*

Table 2 (*continued*)

| GRB Name | z_{est} | T_{90} (s) | $\log F_X$ (erg cm $^{-2}$ s $^{-1}$) | S (15–150 keV) (10 $^{-7}$ erg cm $^{-2}$) | $\log (T_{\text{a}}/10^3)$ (s) | $\log (L_X/10^{47})$ (erg s $^{-1}$) | $\log (E_{\gamma,\text{iso}}/10^{53})$ (erg) | α_1 | α_2 |
|-------------|------------------|-----------------|---|--|-----------------------------------|--|---|------------|------------|
| GRB 201209A | 4.99 | 48 | -10.2±0.06 | 140±10 | -0.23±0.15 | 2.21±0.06 | 0.45±0.03 | -0.24±0.1 | 1.08±0.08 |
| GRB 201229A | 0.52 | 53.3 | -11.5±0.17 | 13±2 | 1.29±0.18 | -1.52±0.17 | -2.15±0.07 | 0.3±0.05 | 1.28±0.1 |
| GRB 210104A | 0.54 | 32.06 | -9.39±0.15 | 88±2 | -0.14±0.28 | 0.66±0.15 | -1.27±0.01 | 0.17±0.17 | 1.41±0.12 |
| GRB 210209A | 0.72 | 139.4 | -10.75±0.15 | 24±2 | 0.64±0.1 | -0.4±0.15 | -1.6±0.04 | 0.28±0.06 | 1.39±0.07 |
| GRB 210306A | 0.18 | 9.12 | -9.5±0.05 | 57±1 | 0.09±0.06 | -0.54±0.05 | -2.41±0.01 | 0.31±0.03 | 1.64±0.05 |
| GRB 210514A | 0.57 | 70.21 | -9.38±0.01 | 74±2 | -0.23±0.03 | 0.74±0.01 | -1.26±0.01 | -0.56±0.06 | 1.35±0.02 |
| GRB 211129A | 0.58 | 113.01 | -10.72±0.11 | 23±2 | 0.63±0.11 | -0.52±0.11 | -1.75±0.04 | 0.09±0.08 | 1.52±0.08 |
| GRB 220325A | 1.37 | 3.5 | -11.16±0.2 | 2.9±0.4 | -0.15±0.45 | -0.25±0.2 | -2.34±0.06 | 0.04±0.19 | 1.01±0.11 |
| GRB 220408A | 0.84 | 17.25 | -10.47±0.21 | 12±1 | -0.03±0.26 | 0.04±0.21 | -1.86±0.04 | 0.18±0.15 | 1.49±0.11 |
| GRB 220518A | 5.86 | 12.29 | -10.54±0.08 | 5.7±0.8 | -0.96±0.21 | 1.92±0.08 | -0.73±0.06 | -0.36±0.25 | 1.36±0.09 |
| GRB 070220 | ... | 129 | -11.55±0.17 | 104±2.33 | 1.3±0.09 | ... | ... | 0.97±0.04 | 2.67±0.33 |
| GRB 090728 | ... | 59 | -10.9±0.14 | 10±2 | 0.37±0.14 | ... | ... | 0.09±0.17 | 1.98±0.15 |
| GRB 090807 | ... | 140.8 | -11.92±0.18 | 22±2 | 1.23±0.12 | ... | ... | 0.14±0.12 | 2.52±0.27 |
| GRB 090904A | ... | 122 | -12.15±0.19 | 30±2 | 1.53±0.13 | ... | ... | 0.31±0.07 | 1.8±0.22 |
| GRB 100614A | ... | 225 | -12.57±0.1 | 27±2 | 2.32±0.07 | ... | ... | 0.31±0.07 | 2.9±0.5 |
| GRB 110208A | ... | 37.4 | -11.47±0.16 | 2.7±0.6 | 0.34±0.48 | ... | ... | 0.27±0.24 | 1.3±0.14 |
| GRB 110315A | ... | 77 | -11.52±0.17 | 41±2 | 1.15±0.12 | ... | ... | 0.74±0.05 | 1.6±0.09 |
| GRB 110420A | ... | 11.8 | -10.35±0.06 | 59±2 | 0.35±0.11 | ... | ... | 0±0.08 | 1.2±0.04 |
| GRB 121001A | ... | 147 | -10.17±0.65 | 17±2 | 0.03±0.65 | ... | ... | 0.8±0.16 | 1.7±0.19 |
| GRB 130315A | ... | 233.4 | -12.21±0.2 | 49±2 | 1.49±0.15 | ... | ... | 0.04±0.17 | 1.88±0.39 |
| GRB 130527A | ... | 44 | -9.92±0.1 | 120±4 | -0.09±0.17 | ... | ... | -0.08±0.29 | 1.81±0.15 |
| GRB 130725B | ... | 10 | -10.33±0.07 | 3.9±0.4 | -0.26±0.17 | ... | ... | -0.22±0.15 | 1.07±0.05 |
| GRB 140730A | ... | 41.3 | -11.78±0.41 | 2.8±0.5 | 0.93±0.36 | ... | ... | 0.35±0.1 | 1.45±0.32 |
| GRB 150626A | ... | 144 | -11.56±0.25 | 18±2 | 1.1±0.37 | ... | ... | -0.01±0.13 | 1.18±0.3 |
| GRB 150817A | ... | 38.8 | -10.11±0.31 | 59±1 | 0.13±0.39 | ... | ... | 0.08±0.18 | 1.3±0.08 |

Table 2 *continued on next page*

Table 2 (*continued*)

| GRB Name | z_{est} | T_{90} (s) | $\log F_X$ (erg cm $^{-2}$ s $^{-1}$) | S (15-150 keV) (10^{-7} erg cm $^{-2}$) | $\log (T_{\text{a}}/10^3)$ (s) | $\log (L_{\text{x}}/10^{47})$ (erg s $^{-1}$) | $\log (E_{\gamma,\text{iso}}/10^{53})$ (erg) | α_1 | α_2 |
|-------------|------------------|-----------------|---|--|-----------------------------------|---|---|------------|------------|
| GRB 171102B | ... | 17.8 | -11.17±0.31 | 9.3±1.4 | 0.95±0.21 | ... | ... | 0.35±0.1 | 1.97±0.38 |
| GRB 180620A | ... | 23.16 | -10.68±0.06 | 58±2 | 0.94±0.03 | ... | ... | 0.06±0.06 | 3.32±0.24 |
| GRB 180925A | ... | 81.7 | -10.76±0.33 | 41±3 | -0.05±0.71 | ... | ... | 0.35±0.12 | 1.55±0.25 |
| GRB 200906A | ... | 70.9 | -11.51±0.39 | 28±1 | 0.84±0.46 | ... | ... | 0.26±0.12 | 1.14±0.2 |
| GRB 220319A | ... | 6.44 | -11.3±0.13 | 2.3±0.4 | 0.09±0.08 | ... | ... | 0.03±0.17 | 3.44±0.53 |
| GRB 220403B | ... | 27 | -11.3±0.17 | 37±1 | 0.94±0.19 | ... | ... | 0.06±0.07 | 1.32±0.13 |
| GRB 220430A | ... | 43.1 | -10.61±0.23 | 440±5 | 0.84±0.13 | ... | ... | 0.88±0.03 | 1.72±0.07 |